AD-A076 018 PENNSYLVANIA STATE UNIV UNIVERSITY PARK F/G 4/1
A HIGH SPEED DIGITAL AUTOCORRELATOR AND ITS APPLICATION TO MESO--ETC(U)
JUL 79 P T PETRUNO , J J OLIVERO DAAG29-78-G-0083
UNCLASSIFIED ERADCOM/ASL-CR-79-0083-1 NL

1 OF 2
AD
A076018

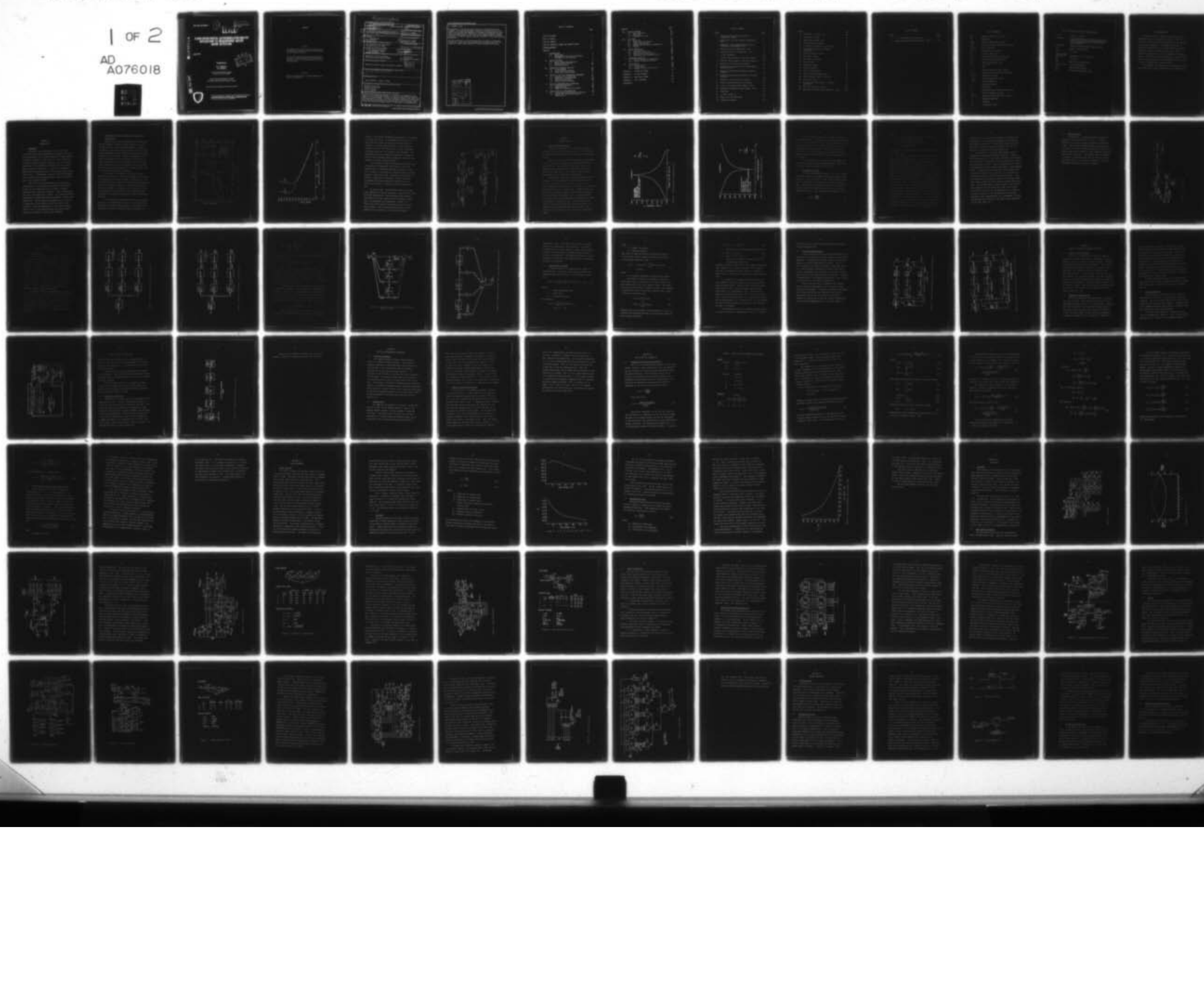

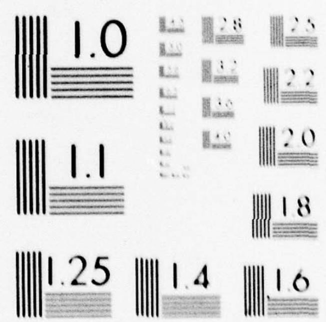

MICROCOPY RESOLUTION TEST CHART
NATIONAL BUREAU OF STANDARDS-1963-A

ASL-CR-79-0083-1

12

A HIGH SPEED DIGITAL AUTOCORRELATOR AND ITS APPLICATION TO MESOSPHERIC WATER VAPOR DETECTION

July 1979

Prepared by

P.T. Petruno
J.J. Olivero

The Pennsylvania State University
University Park, PA 16802

Under Contract DAAG29G-78-G-0083
CONTRACTOR MONITOR: Robert O. Olsen

Approved for public release; distribution unlimited

U.S. ARMY
ERADCOM

US Army Electronics Research and Development Command
ATMOSPHERIC SCIENCES LABORATORY
White Sands Missile Range, NM 88002

NOTICES

Disclaimers

Disposition

(18) ERADCOM/ASL

SECURITY CLASSIFICATION OF THIS PAGE (When Data Entered)

(19) REPORT DOCUMENTATION PAGE		READ INSTRUCTIONS BEFORE COMPLETING FORM
1. REPORT NUMBER ASL-CR-79-0083-1	2. GOVT ACCESSION NO.	3. RECIPIENT'S CATALOG NUMBER (9)
4. TITLE (and Subtitle) (6) A HIGH SPEED DIGITAL AUTOCORRELATOR AND ITS APPLICATION TO MESOSPHERIC WATER VAPOR DETECTION		5. TYPE OF REPORT & PERIOD COVERED Technical Report 6. PERFORMING ORG. REPORT NUMBER
7. AUTHOR(s) (10) P. T. Petruno and John J. Olivero		8. CONTRACT OR GRANT NUMBER(s) (15) DAAG29G-78-G-0083 New
9. PERFORMING ORGANIZATION NAME AND ADDRESS The Pennsylvania State University University Park, PA 16802		10. PROGRAM ELEMENT, PROJECT, TASK AREA & WORK UNIT NUMBERS DA Task No. 1L161102B53A/SA2
11. CONTROLLING OFFICE NAME AND ADDRESS US Army Electronics Research and Development Command Adelphi, MD 20783		12. REPORT DATE (11) July 1979 13. NUMBER OF PAGES 113
14. MONITORING AGENCY NAME & ADDRESS(if different from Controlling Office) Atmospheric Sciences Laboratory White Sands Missile Range, NM 88002		15. SECURITY CLASS. (of this report) UNCLASSIFIED 15a. DECLASSIFICATION/DOWNGRADING SCHEDULE
16. DISTRIBUTION STATEMENT (of this Report) Approved for public release; distribution unlimited (12) 125		
17. DISTRIBUTION STATEMENT (of the abstract entered in Block 20, if different from Report) (16) 1L161102B53A		
18. SUPPLEMENTARY NOTES Contract Monitor: Robert O. Olsen		
19. KEY WORDS (Continue on reverse side if necessary and identify by block number) Mesosphere water vapor Digital autocorrelator Spectral analysis 22 GHz radiometer		
20. ABSTRACT (Continue on reverse side if necessary and identify by block number) The emission and absorption spectrum of stratospheric and mesospheric water vapor are to be detected and analyzed. In both cases the method of detection requires a 22 GHz radiometer, and the data analysis requires a high speed, high resolution spectral analyzer. The basic radiometer fundamentals are discussed here, then the various techniques of spectral analysis are considered, which include both digital and analog versions of filter banks and autocorrelators. cont →		

DD FORM 1473, 1 JAN 73 EDITION OF 1 NOV 65 IS OBSOLETE

278650

SECURITY CLASSIFICATION OF THIS PAGE (When Data Entered)

20. ABSTRACT (cont)

Cont

A prototype 2 x 1 bit digital autocorrelator was then designed and constructed. The system was designed to operate at a sampling rate of up to 100 MHz, with a resolution dependent on the number of autocorrelation points used. The system was then interfaced to a Nova 1200 minicomputer for data accumulation and transfer of data to nine track magnetic tape for standard processing. An IBM 370 computer system was available for final data reduction and analysis.

The final system was a 16 point autocorrelator, two points of which were constructed. Future goals include completing the 16 points and using the system for a ground based measurement of upper atmosphere water vapor.

TABLE OF CONTENTS

LIST OF FIGURES

LIST OF TABLES

LIST OF SYMBOLS

$A(x)$	Normal probability function
BW	Bandwidth
F_{DSB}	Double sideband noise figure
P_{dr}	Bivariate normal probability function
$P(i\sigma f)$	Power spectrum
$R(i\Delta\tau)$	Autocorrelation function
Ta	Antenna temperature
Te	Equivalent receiver temperature
Top	System operating temperature
Vo	Sampling threshold level
$Z(x)$	$\frac{1}{\sqrt{2\pi}} e^{-x^2/2}$
n	Autocorrelation product weight
$r(i\Delta\tau)$	Normalized autocorrelation estimate
$w(n\Delta\tau)$	Weighting function
ΔT_{min}	Minimum detectable signal
Δf, ΔF	Filter bandwidth
Δt	Sampling interval
$\Delta\tau$	Unit delay
α	Coefficient describing receiver type
σf	Filter frequency spacing
$\rho(i\Delta\tau)$	Normalized autocorrelation function
σ	Standard deviation
σ^2	Variance
τ_I	Integration time

LIST OF TECHNICAL TERMS AND ABBREVIATIONS

A to D	Analog to digital
Aliasing	Error introduced in the Fourier Analysis of sampled data by which frequencies too high to be analyzed contribute to lower frequency amplitude
Crosstalk	Signal transfer between parallel lines
ECL	Emitter Coupled Logic
GHz	10^9 Hertz
Gross or Hard Quantization	Quantizing to 3 or less bits
MHz	10^6 Hertz
MOS	Metal Oxide Semiconductor
Nyquist rate	Two times bandwidth
RAM	Random Access Memory
TTL	Transistor-Transistor Logic

ACKNOWLEDGMENTS

The author wishes to express his appreciation to Professors Leslie C. Hale, John J. Olivero, and John B. Lewis for their many helpful discussions and for serving as his thesis committee. The author also wishes to express his gratitude to Dr. Charles Croskey who contributed much time and knowledge to this work, and is presently constructing the 22 GHz radiometer discussed herein. Also of great assistance were Dr. John S. Nisbet and many other members of the Ionosphere Research Laboratory at The Pennsylvania State University.

This research was supported by the Department of the Army under grant number DA AERO-4400 and DA MINCON-4502.

CHAPTER I

INTRODUCTION

1.1 Background

Mesospheric and stratospheric water vapor have historically been elusive quantities to measure, and yet such measurements are of prime importance in understanding atmospheric processes. Water vapor is a key constituent in many atmospheric chemical reactions, and is of obvious importance to ice nucleation processes with their consequent release of latent heat. A variety of atmospheric models have been developed with widely varying water vapor mixing ratios. Measurements, moreover, have been plagued with uncertainties since the earliest attempts at measurement in the nineteen forties.

The first in-situ measurements were suspected of contamination by the measuring instruments and balloons. During the late nineteen fifties, methods of remotely measuring water vapor were attempted. Remote measurements were free of contamination, however, the increase difficulty encountered in conducting remote measurements lowered their credibility. Current remote measurements vary as much as 75 ppm whereas current models allow only about 10 ppm variation. Thus the measurement of high altitude water vapor is still in the research phase and should improve greatly with advances in theory and technology.

1.2 Experimental Outline and General Statement of the Problem

Remote water vapor measurements take advantage of the H_2O molecule's natural resonant properties in the microwave portion of the frequency spectrum. Figure 1 (Longbothum, 1976) shows three resonances of water vapor and how atmospheric oxygen raises the apparent background radiation about each line. Figure 2 (Longbothum, 1976) shows the apparent pressure broadening occurring in the lower altitudes for the 22 and 183 GHz lines. The line shape reveals not only an approximate water vapor mixing ratio, but may provide mixing ratio versus altitude data if suitable data analysis is employed.

Two types of measurements are considered here, emission and absorption. Resonant emissions are detected by observing the atmosphere against a background, as free as possible of other sources, by looking away from galactic sources. Resonant absorption is detected by observing a hot source beyond the atmosphere, most generally the sun. The intervening water vapor will then absorb radiation according to its mixing ratio and the relative atmospheric pressure.

It was decided to detect the water vapor resonance centered at 22.23507985 GHz, since this is the only line which may be studied from the ground. Although the peak amplitude at 22 GHz is relatively small, according to

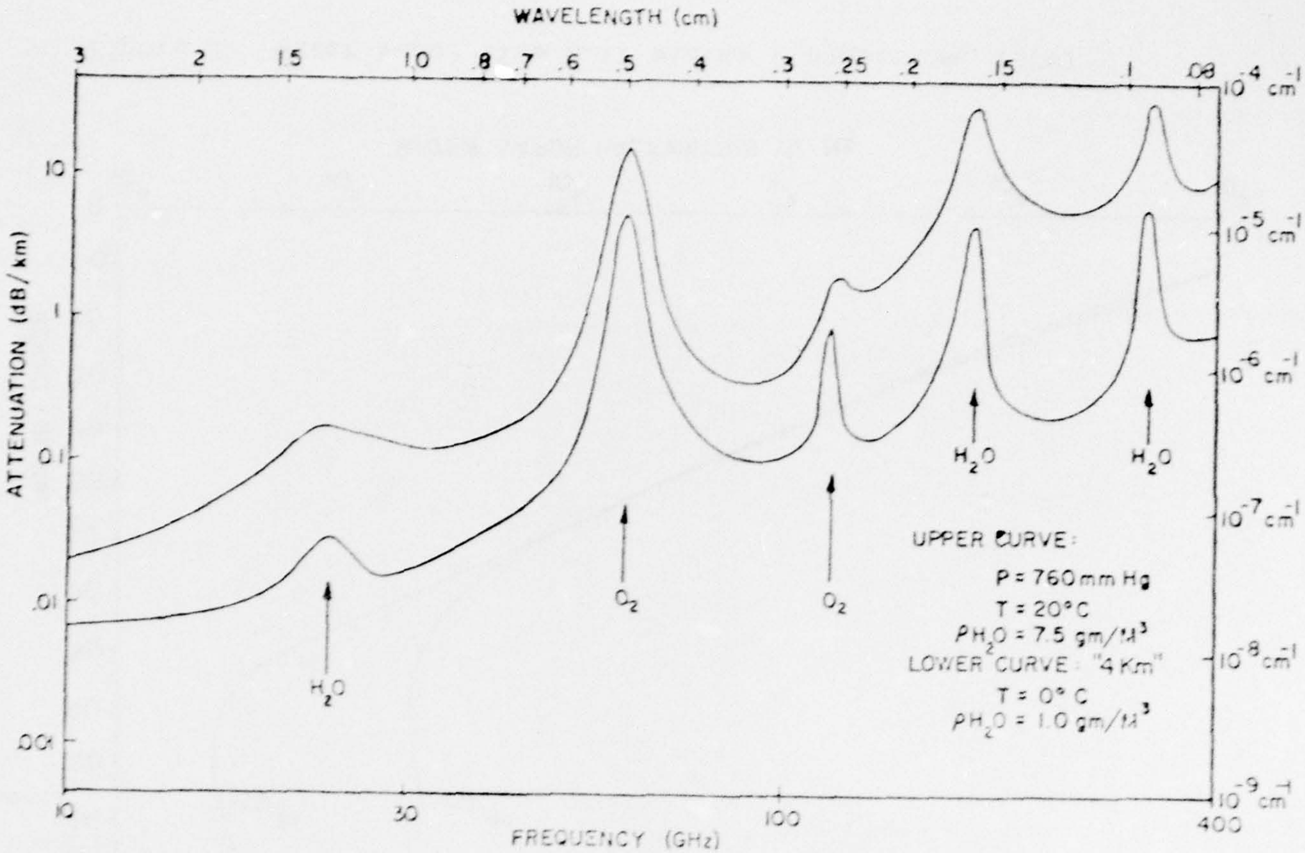

Figure 1. Atmosphere absorption coefficient (Longbothum, 1976)

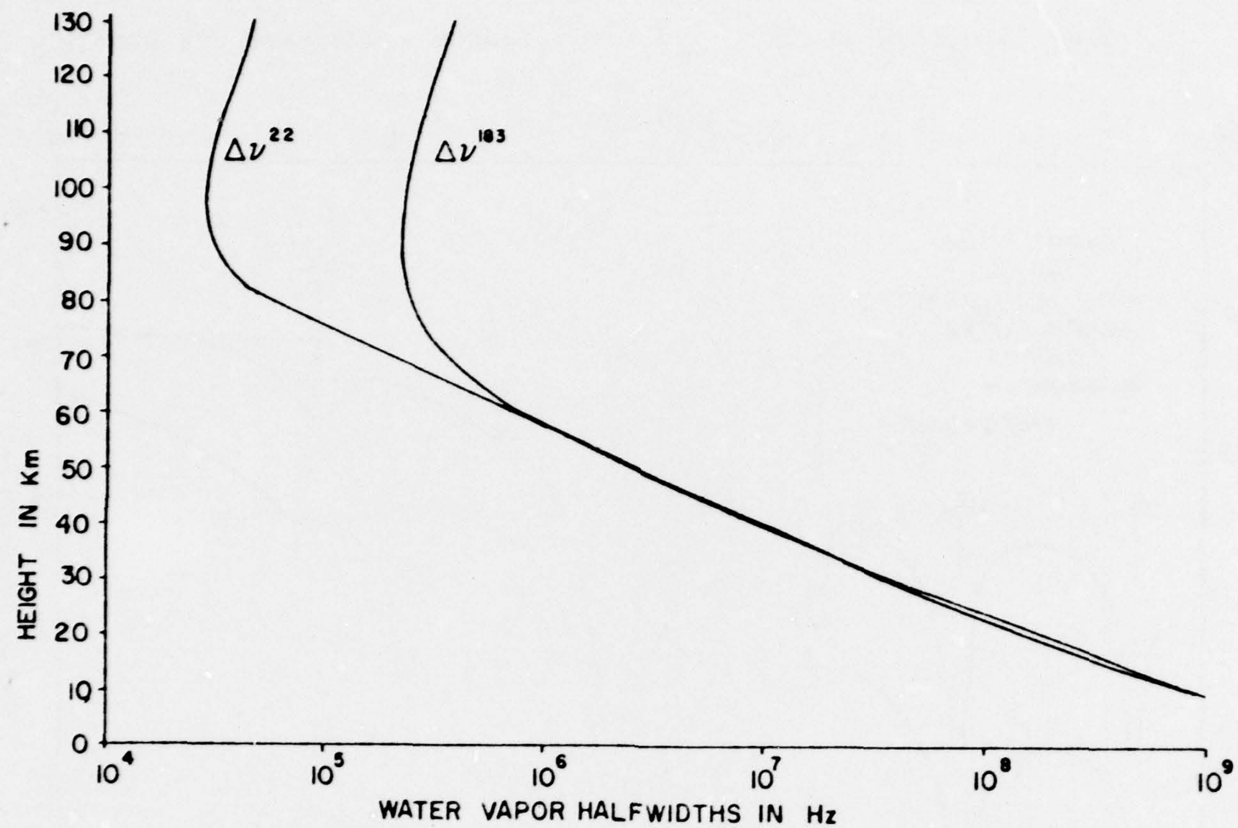

Figure 2. Water vapor line half widths (Longbothum, 1976)

Figure 1, the overall atmospheric attenuation is also small. At 183 GHz and above, the atmospheric absorption is so great that the higher altitude contribution would be unusable to a ground based detector. Other attractive features of the 22 GHz line are its relative remoteness from other lines and its relatively low frequency. The remoteness will cause least bias from other resonances, and the lower frequency employs components which are less expensive and more readily available.

An instrument capable of detecting the 22 GHz line was proposed by Longbothum (1976) and has since been improved upon. Longbothum describes a microwave radiometer (Figure 3) consisting of a super heterodyne receiver feeding a large filter bank. Each filter then feeds a detector, integrator, and analog to digital converter. A computer would then periodically sample the A to D outputs and continue to compile and finally reduce the data.

In recent times, autocorrelators have been extensively employed as spectral analyzers, especially for radio astronomy applications. Autocorrelators have inherent advantages over filter banks as will be discussed herein. Thus, an improvement over Longbothum's scheme is to replace the filter bank and associated circuitry with an autocorrelator. The implications and analysis of this change will be described in the following chapters.

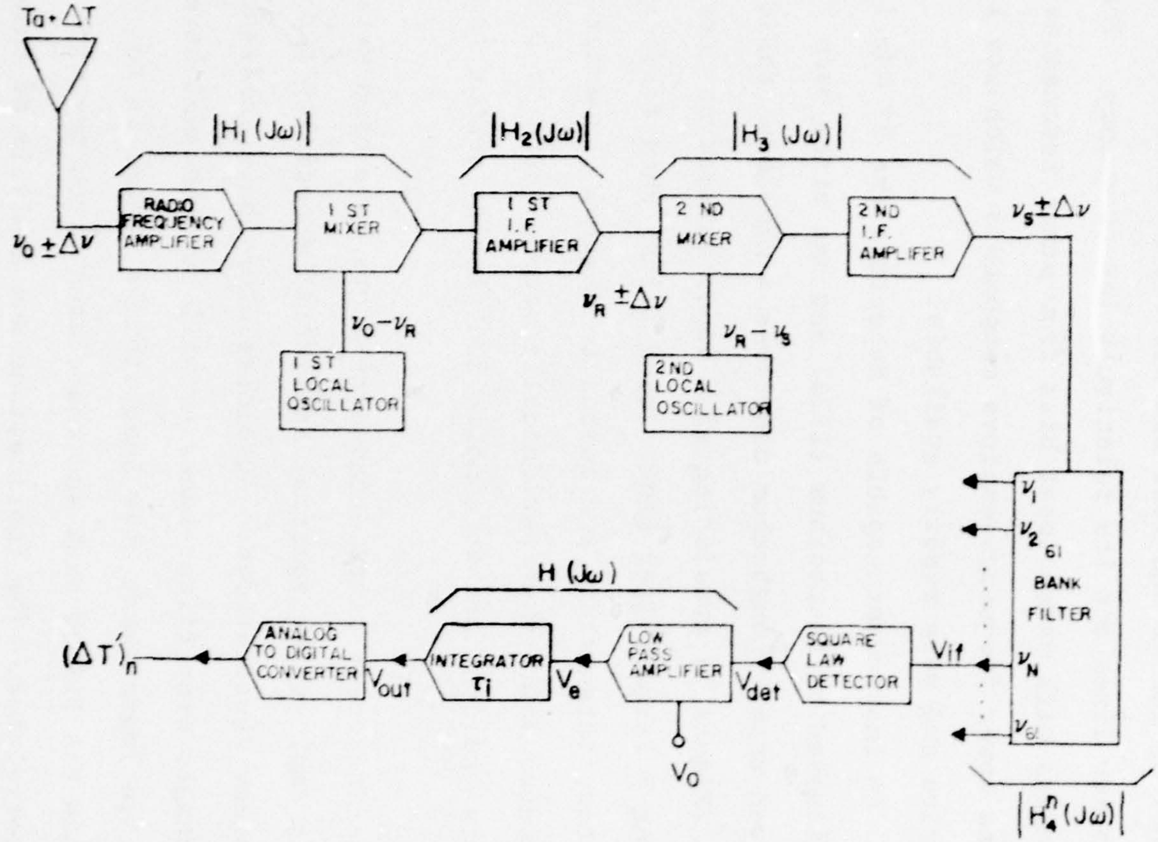

Figure 3. Mesospheric and stratospheric microwave radiometer (Longbothum, 1976)

CHAPTER II

DESIGN CRITERIA

2.1 Basic System Requirements

A system is needed that will detect the spectral content of the water vapor line centered at 22.23507985 GHz. The desired altitude of the line will be from approximately 40 km up.

Figure 2 shows that the line halfwidth corresponding to 40 km is 10 MHz. The necessary system bandwidth then becomes 20 MHz. This bandpass effectively reduces the lower altitude information to an approximate DC bias on the high altitude curve. This permits a high altitude measurement from a ground based observation.

Although this report will not be concerned with RF hardware, a brief description of overall system sensitivity and calibration will be required. Figures 4 and 5 are a theoretical representation of the water vapor emission and absorption spectra, respectively. These have been derived from a computer simulated, ground based observation of the atmosphere (Longbothum, 1977). As was mentioned previously, water vapor measurements vary greatly and thus the atmospheric models vary also. These simulations are based on only one such model and should therefore be considered only as guidelines for a system design. This model and others are more fully described in Longbothum's report.

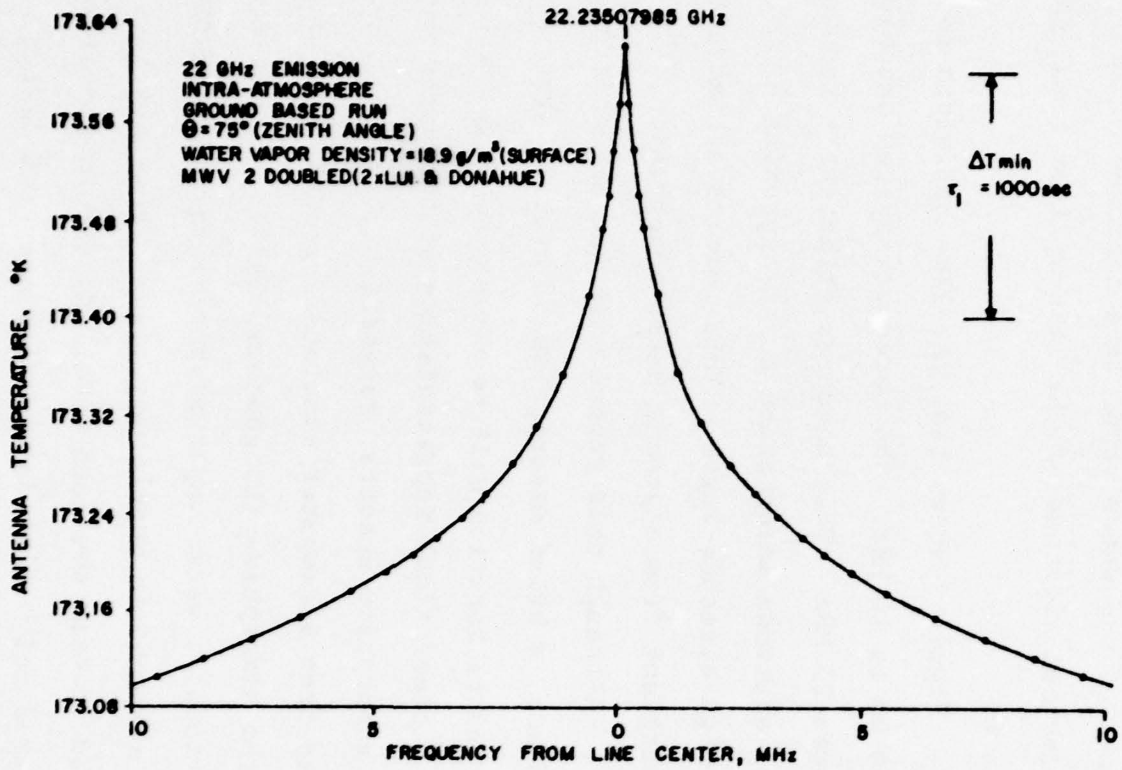

Figure 4. Emission spectra (Longbothum, 1977)

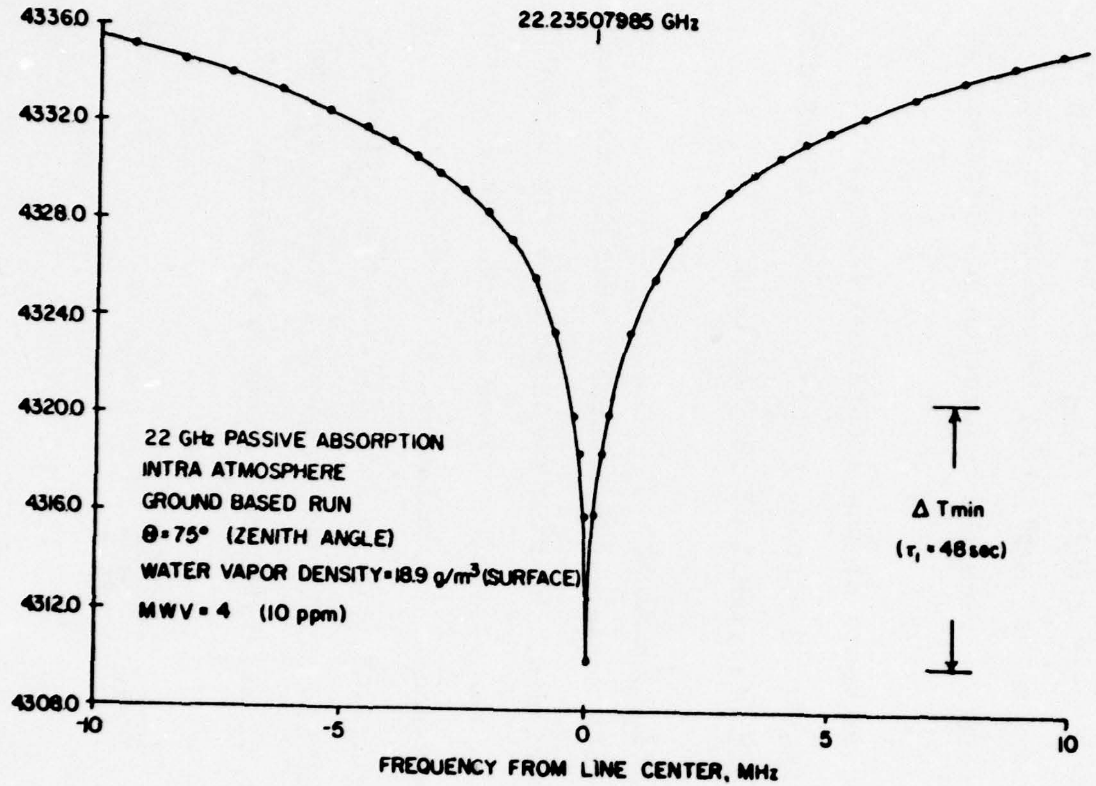

Figure 5. Absorption spectra (Longbothum, 1977)

These simulations, however, do suggest overall system sensitivities. For the emission experiment, temperatures of 173 K must be received with a system sensitivity to signals 0.5 K or less. This sensitivity will be defined as the minimum detectable signal, ΔT_{min}. Although ΔT_{min} is given here as the signal amplitude, in practice a much smaller ΔT_{min} will be required to provide any accuracy in line shape.

The requirements of the absorption experiment are less severe, requiring antenna temperatures of 4300 K with a minimum detectable signal of 30 K or less.

2.2 Measurement Accuracy

To improve measurement accuracy, that is, to reduce measurement variance, the minimum detectable signal should be made as small as possible. These extreme sensitivities can be accomplished by accumulating the desired signal in time. The following relationship defines the radiometer's minimum detectable signal when viewing a thermal source. (Adapted from Tiuri, 1964, and O'Kean and Lombardo, 1973.)

$$\Delta T_{min} = \frac{\alpha Top}{\sqrt{BW\tau_I}} \qquad (1)$$

Where:

α = Coefficient describing type of receiver

BW = High frequency bandwidth

Top = System operating temperature

τ_I = Integration time

The ΔT_{min} here is equivalent to the standard deviation of the received power.

When viewing a thermal source over time, amplifier gains may vary somewhat, making a calibration step essential. The Dicke radiometer (Dicke, 1946) mechanically switches the radiometer to a standard noise source 30 times per second. This rapid transition gives a reference signal often enough to reduce gain variations. An alternative to Dicke switching is frequency switching. In this method the local oscillator frequency is switched such that the radiometer is looking off line to a flat portion of the spectrum. Then, by accumulating the difference between the on and off frequency measurements a relative spectrum may be determined, independent of receiver or signal DC characteristics. Then, to achieve a true record of receiver gain variations, a waveguide switch is used to switch from the antenna to a reference noise source. These two references and the signal measurement must then be taken before the receiver gain varies. Thus, the switching time must be short but also long enough to make the receiver local

oscillator lock up time and the waveguide switching time insignificant. A reasonable measurement period would be one second in each mode. The spectral analyzer must then cope with the various calibrating signals over the time necessary to achieve the desired sensitivity.

The accuracy of the water vapor mixing ratios is dependent on the measured spectral resolution. That is, each spectral point is a function of frequency and altitude, and can be used to determine the water vapor mixing ratio at that particular altitude. This is accomplished by solving the radioactive transfer equation developed by Chandrasekhar (1960). Determining the actual water vapor mixing ratios is beyond the scope of this paper but is given some consideration by Waters (1976) and Longbothum (1976). Spectral resolution, then, greatly affects the resultant water vapor mixing ratios and will eventually require much attention. The optimum number of points required, the centers and bandwidths are also beyond the scope of this paper. A sufficient criterion for the purposes here is simply to provide as accurate a line representation as possible. Included in that representation is a requirement of having one spectral point located at the exact center frequency of the water vapor line.

2.3 Design Criteria

In conclusion, the desired spectral analyzer is required to analyze a band 20 MHz wide. To prevent aliasing, this allows a center frequency no lower than 10 MHz. The receiver minimum detectable signal must be less than 0.5 K, and the spectral analyzer is required to remain stable for the amount of time necessary to achieve the desired sensitivity. The analyzer then is required to produce a calibrated power spectrum over the 20 MHz band with emphasis at the center frequency. The basic radiometer now appears as shown in Figure 6.

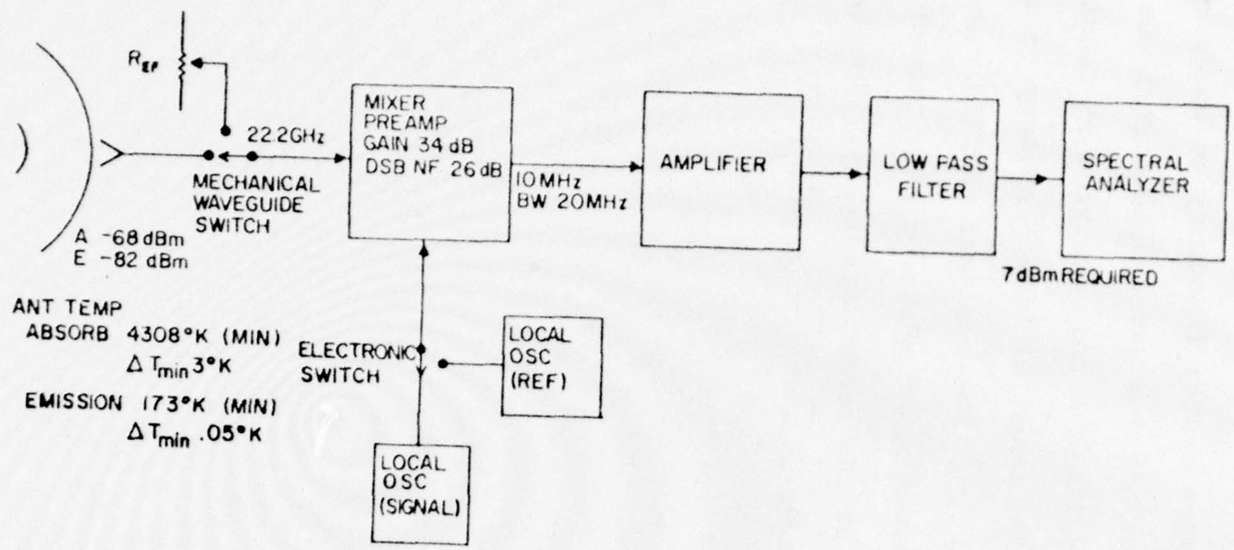

Figure 6. 22 GHz radiometer

CHAPTER III

METHODS OF SPECTRAL ANALYSIS

3.1 Filter Method

Power spectra, basically, can be effectively measured using two different techniques. (Another method, the swept frequency or "spectrum analyzer" technique, sacrifices too much of the available information to be seriously considered.) The first technique, as was suggested by Longbothum, involves dividing the signal through a bank of bandpass filters. The filter outputs are then squared and averaged in time to provide the power spectrum. This method can be accomplished using either digital or analog circuitry, or combinations of the two. The basic digital and analog circuits are shown in Figures 7 and 8, respectively.

The analog method is straightforward, however, in order to realize the scope of digital requirements, the digital filter deserves somewhat further explanation. The most general method of implementing digital filters is the recursive realization. That is, a filter whose transfer function includes both poles and zeros, as described here in terms of the z-transform (Rabiner and Gold, 1975).

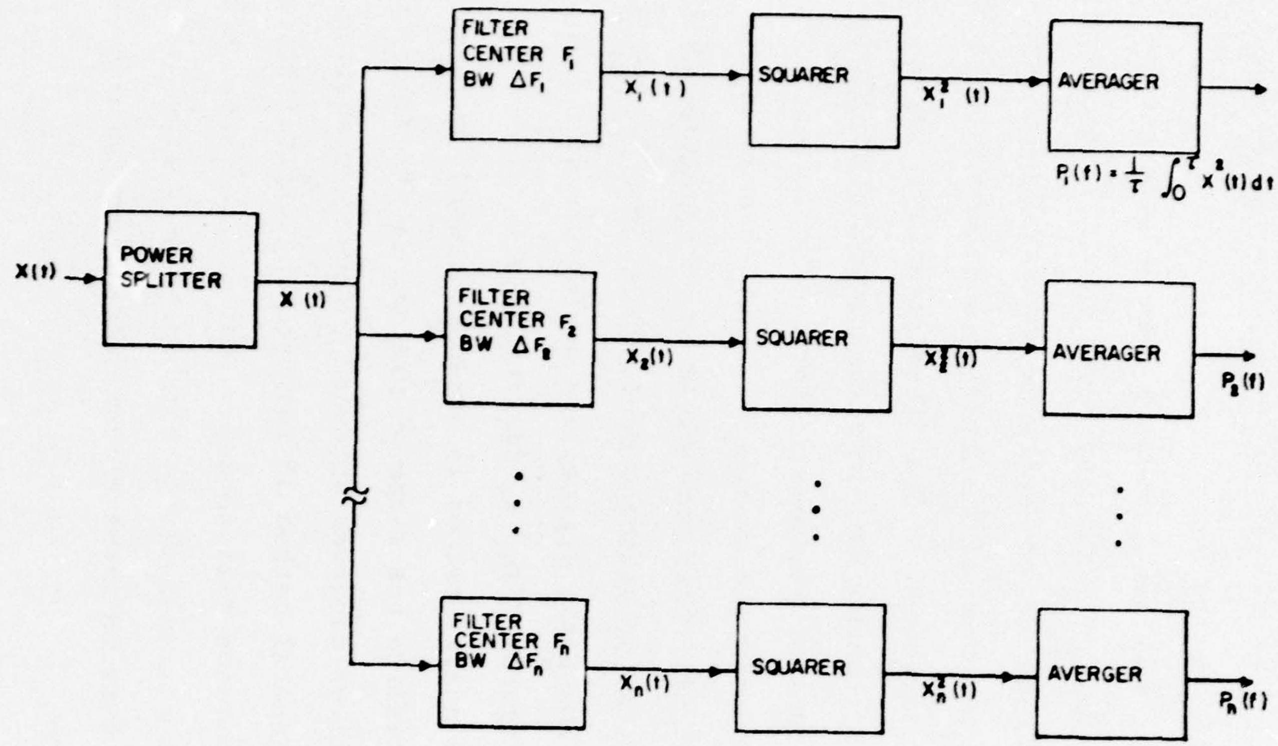

Figure 7. Analog filter method of spectral analysis

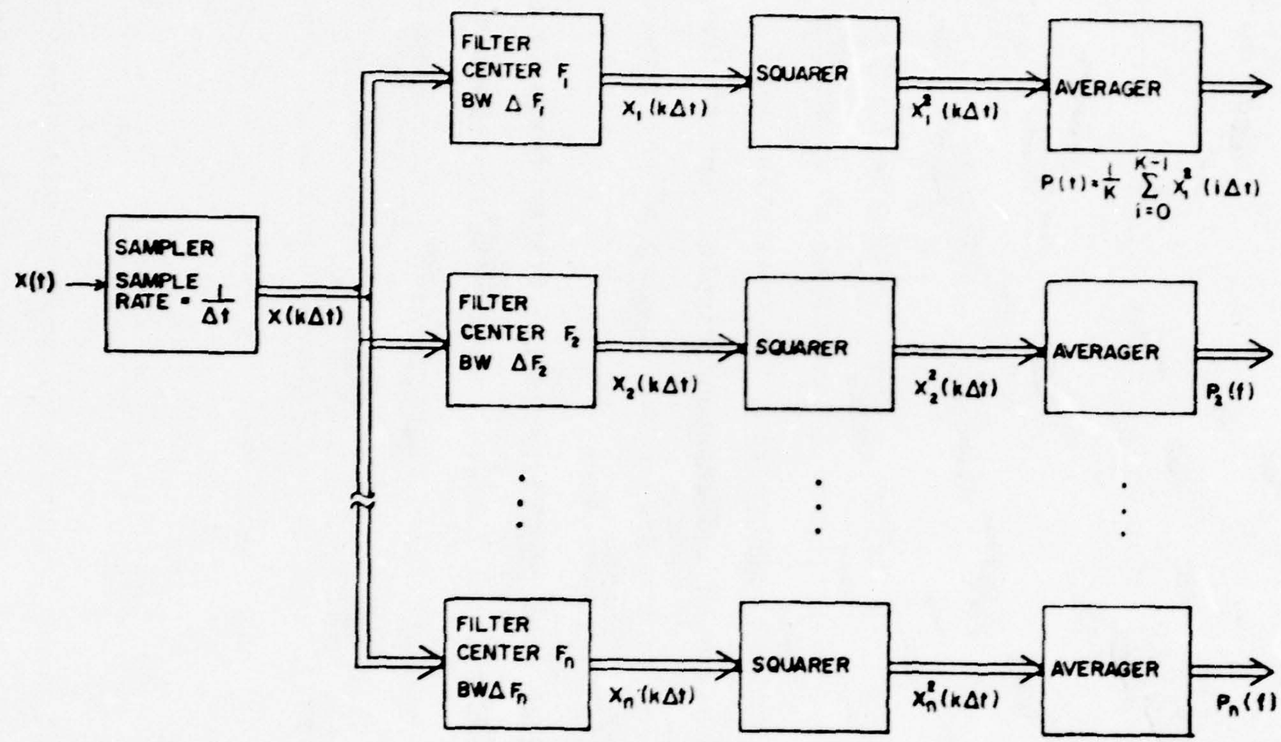

Figure 8. Digital filter method of spectral analysis

$$H(z) = \frac{Y(z)}{X(z)} = \frac{\sum_{i=0}^{N} a_i z^{-i}}{\sum_{i=0}^{N} b_i z^{-i}} \quad (2)$$

The difference equation is then derived using the inverse z-transform:

$$y(n) = \sum_{i=0}^{N} a_i x(n-i) - \sum_{i-1}^{N} b_i y(n-i) \quad (3)$$

A realization of this filter is shown in Figure 9. The number of delays is analogous to the order of an analog filter, predominantly controlling the transition band phase and the passband and stopband ripple. Cutoff frequencies are set by the proper combination of the sampling rate and multiplying constants.

A special case of the recursive filter leads to a second class of digital filters, namely the nonrecursive filters. These filters are characterized by having poles at z=0 only, that is, the denominator of Equation (2) is equal to 1. This leads to a difference equation as shown in Equation (4), and a realization as shown in Figure 10.

$$y(n) = \sum_{i=0}^{N} a_i x(n-i) \quad (4)$$

Both of these filters are discussed extensively in a variety of textbooks (Rabiner and Gold, 1975, Oppenheim

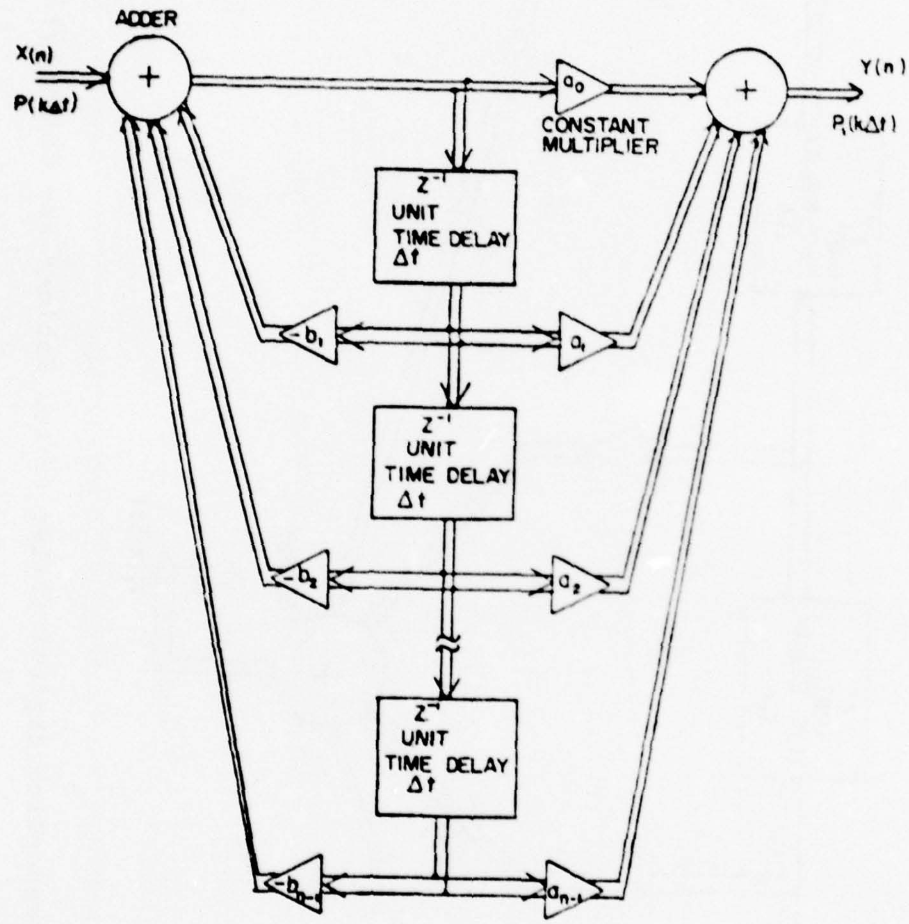

Figure 9. Recursive digital filter (after Rabiner and Gold, 1977)

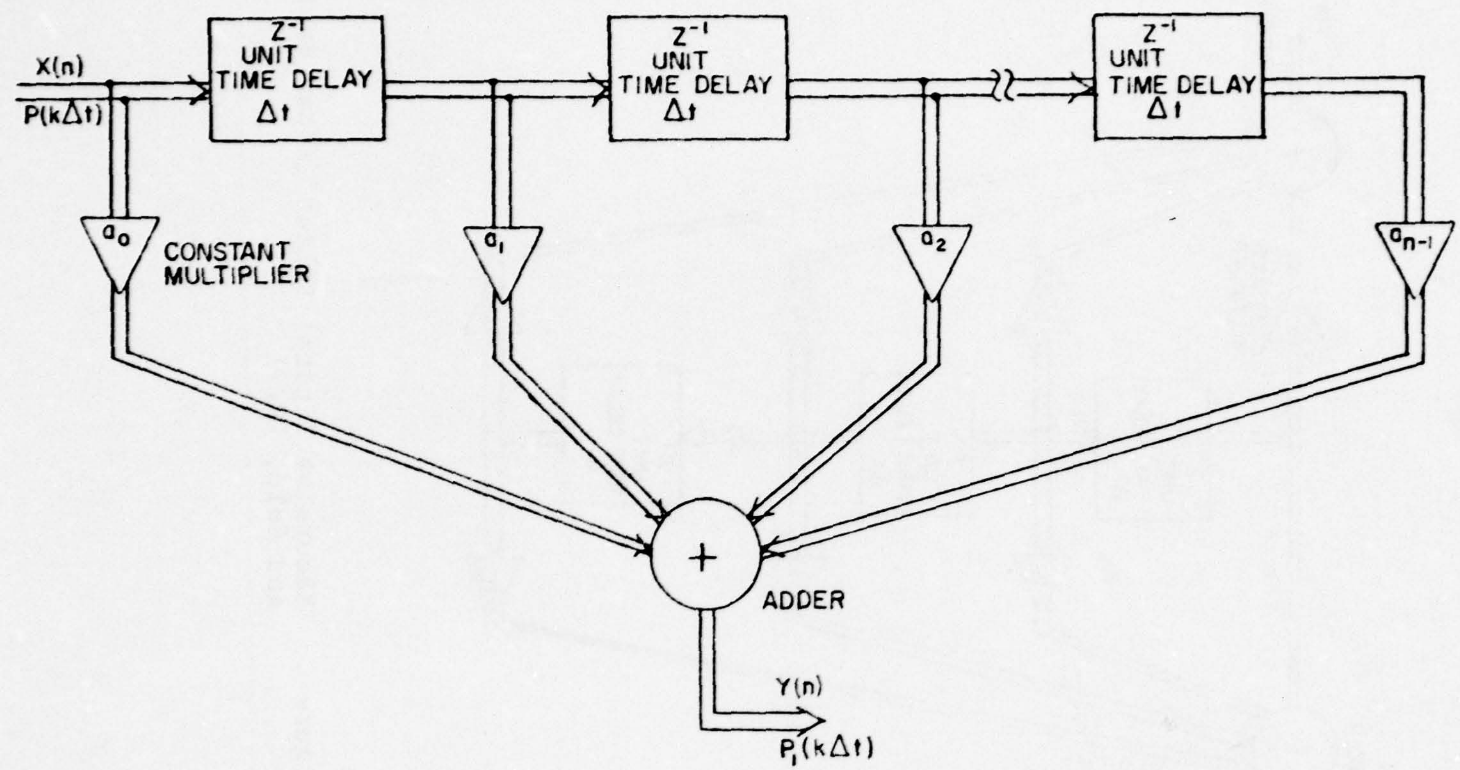

Figure 10. Nonrecursive digital filter (after Rabiner and Gold, 1977)

and Schafer, 1975). The intent here is only to attain a feel for the complexity of the circuitry. An important consideration is the fact that for a given filter transfer function, the likelihood of obtaining integer values of a_i and b_i is negligible. This means that either a complex multiplier is required or the intended filter characteristics must be sacrificed.

3.2 Autocorrelation Method

A second technique for measuring power spectra is autocorrelation. The basic autocorrelator performs the autocorrelation function, $R(i\Delta\tau)$, on the incoming signal, $x(t)$.

$$R(i\Delta\tau) = \frac{1}{T}\int_0^T x(t)x(t+i\Delta\tau)dt; \; i=0,1,2,\ldots,N-1 \qquad (5)$$

Where:

T = Total correlation time

$\Delta\tau$ = Unit delay

N = Correlation points

or digitally;

$$R(i\Delta\tau) = \frac{1}{K}\sum_{k=0}^{k-1} x(k\Delta t)x(k\Delta t+i\Delta\tau); \quad i=0,1,2,\ldots,N-1 \qquad (6)$$

Where:

K = Number of products

Δt = Sampling interval

The result is then multiplied by a weighting function, $w(\gamma)$, and the Discrete Fourier Transform is performed on the products (Weinreb, 1963).

$$P(i\delta f) = 2\Delta\tau R(o)w(o) + 4\Delta\tau \sum_{n=1}^{N-1} R(n\Delta\tau)w(n\Delta\tau)\cos(2\pi i\delta f n\tau) \quad (7)$$

Where:

δf = Frequency difference between filter centers.

The weighting function is required to make the result here equal to the result of a discrete filter output (Schwartz and Shaw, 1975, Weinreb, 1963). The analog form of the filter output is shown in Figure 7 and repeated in Equation (8), while its equivalent digital form is shown in Figure 8 and Equation (9).

$$P(\delta f) = \frac{1}{T}\int_o^T x^2(t)dt \quad (8)$$

$$P(\delta f) = \frac{1}{K}\sum_{k=0}^{K-1} x^2(k\Delta t) \quad (9)$$

Weinreb shows an equivalence between Equations (5) and (7), providing the weighting function is any function exhibiting the following conditions:

$$\text{(a)} \quad w(o) = 1 = \int_{-\infty}^{\infty} W(f)df \qquad (10)$$

Where W(f) is the fourier transform of w(o);

$$\text{(b)} \quad w(n\Delta\tau) = w(-n\Delta\tau) \qquad (11)$$

$$\text{(c)} \quad w(n\Delta\tau) = 0 \text{ for } |n| \geq N \qquad (12)$$

Where N is the number of delays used in the autocorrelation function.

A number of weighting functions are in common use (Weinreb, 1963, Hamming, 1977, Schwartz and Shaw, 1975), however, according to Blackman and Tukey (1958), the choice of window does not considerably influence the resulting spectrum.

A disadvantage in using autocorrelators over the filter method of spectral analysis is in the spacing between frequency points. Weinreb (1963) shows that evenly spaced delays result in evenly spaced spectral points. That spacing, δf, corresponds to $1/N\Delta\tau$, where N is the number of autocorrelation delays and $\Delta\tau$ is the unit delay time. The half power bandwidth, Δf, of each spectral point will be approximately $2\delta f$. Obviously then, as N is reduced, the spectral points become more spread out over the band, but wider in bandwidth.

Autocorrelators can also be implemented using analog or digital circuitry or combinations of the two. Figures

11 and 12 show in block form the basic functions required for each implementation.

3.3 Power Spectrum Estimate

A note should also be made that the methods of spectral analysis described here do not provide the exact power spectrum. To determine the average power of a stochastic signal, an infinite time would be required. That is, T and K would need to approach infinity in Equations (8) and (9). Experimentally obtaining an infinite time record is not a reasonable idea, and thus, a truncated, or estimate, version of the power spectrum is accepted. A measure of uncertainity in the spectral measurement is the variance or sensitivity, and is shown in Equation (1).

Again, the idea here in presenting the different forms of spectral measurement is not to provide a vast theoretical background. A rigorous theoretical development can be found in many of the references listed, and in particular, from a most basic form in Lewis (1977). Instead, the intent was to show the relative complexities in the various implementations of a spectral analysis.

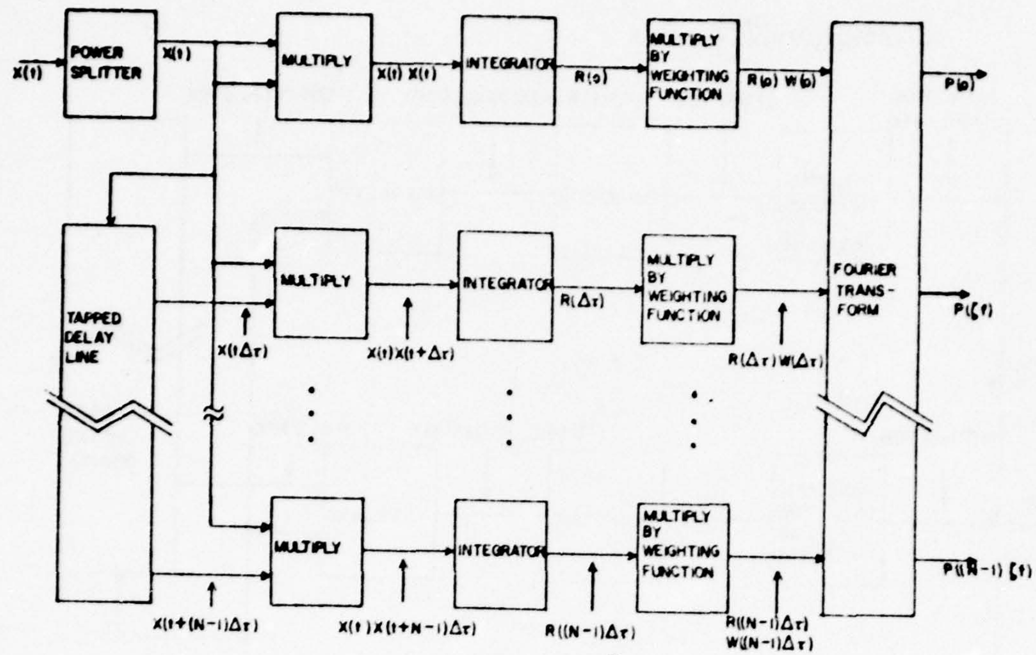

$$R(i\Delta\tau) = \frac{1}{T}\int_0^T X(t)\,X(t+i\Delta\tau)\,dt$$

Figure 11. Analog autocorrelation method of spectral analysis

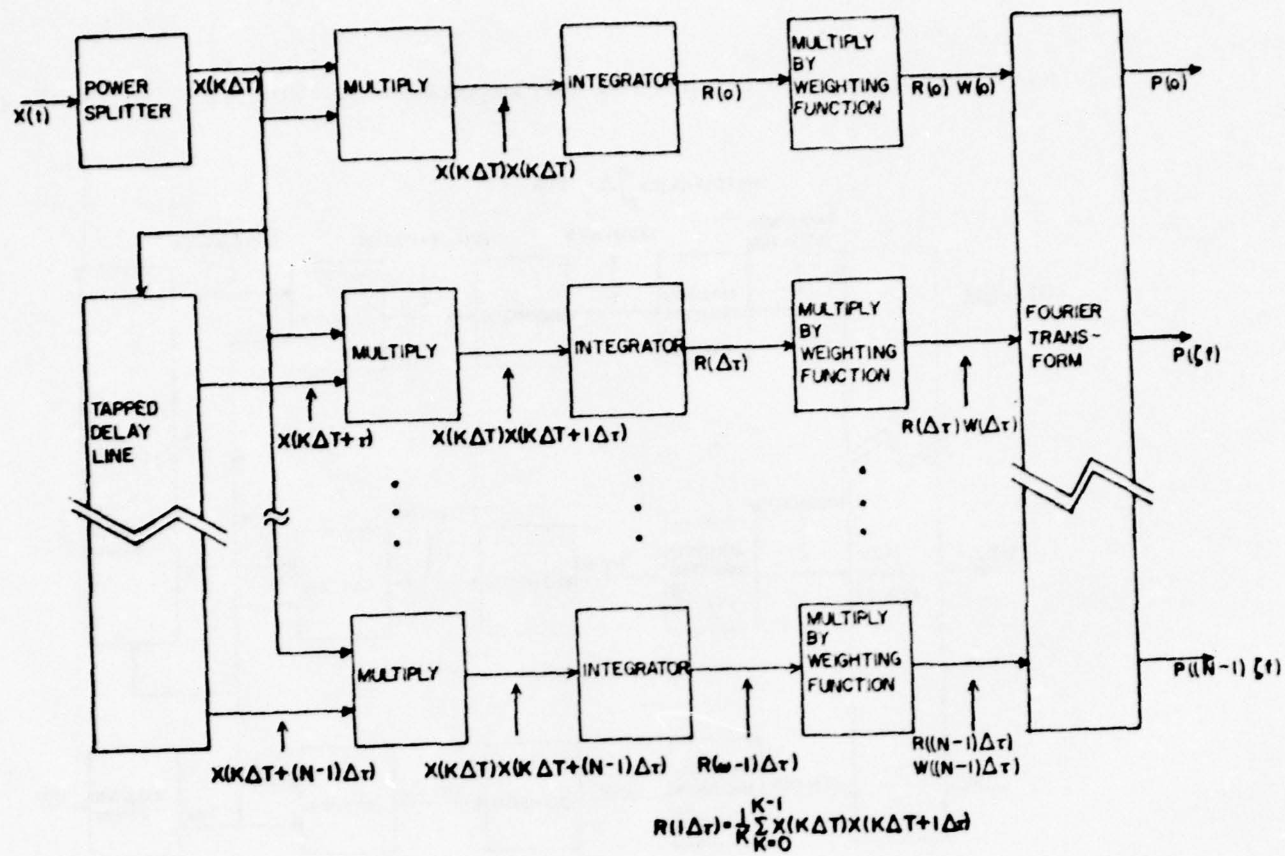

Figure 12. Digital autocorrelation method of spectral analysis

CHAPTER IV

CHOICE OF SPECTRAL ESTIMATION TECHNIQUE

4.1 Stability Considerations

The basic considerations in choosing a spectral estimation technique are stability, complexity, and cost. Stability becomes a problem in analog circuitry. Amplifier and multiplier gains must be kept constant. Filter center frequencies and bandwidths must be kept constant. Also integrator time constants and delay line delay times must remain constant. These variables must not only remain constant over integration times on the order of hours, but must also remain equivalent from channel to channel for perhaps tens of channels. The major stability concern for the digital circuitry stems from keeping the sampling interval constant. This requires only a single oscillator to remain stable over time.

4.2 Bandwidth Considerations

The 20 MHz bandwidth requirement makes the digital circuitry difficult. High speed circuitry must be used, thus timing becomes critical. Also gate delays, crosstalk, and even transmission line reflections become important. The digital filter method has an additional difficulty, in that to attain proper channel centers and bandwidths, a significant number of bits are required. Therefore, at

least one multibit multiplier is required per channel, and at a Nyquist rate of 40 MHz, the multiplication must be performed in less than 25 nanoseconds. The digital autocorrelator technique alleviates this problem since the autocorrelation function can be performed using as few as one bit. Multiplications now became only an "exclusive or" function and can be performed in one gate delay. This gross quantization error is paid for by a loss of sensitivity. The correlation time must then be lengthened to achieve a sensitivity equal to a multibit autocorrelator or a filter bank.

A 20 MHz bandwidth would not be a difficult procedure for analog circuitry; however, the stability requirements would cause an increase in the circuit complexity and cost.

4.3 Cost Consideration

A good indication of relative cost is found by examining the "front ends" of each spectral estimation technique. The final accumulations in all cases can most easily be done using a digital computer. Therefore, most of the expense and design effort would be expended on the high speed front end of each technique.

A typical block diagram of a recursive digital filter is summarized in Figure 13. The circuit is implementing an 8 bit version of the difference equation:

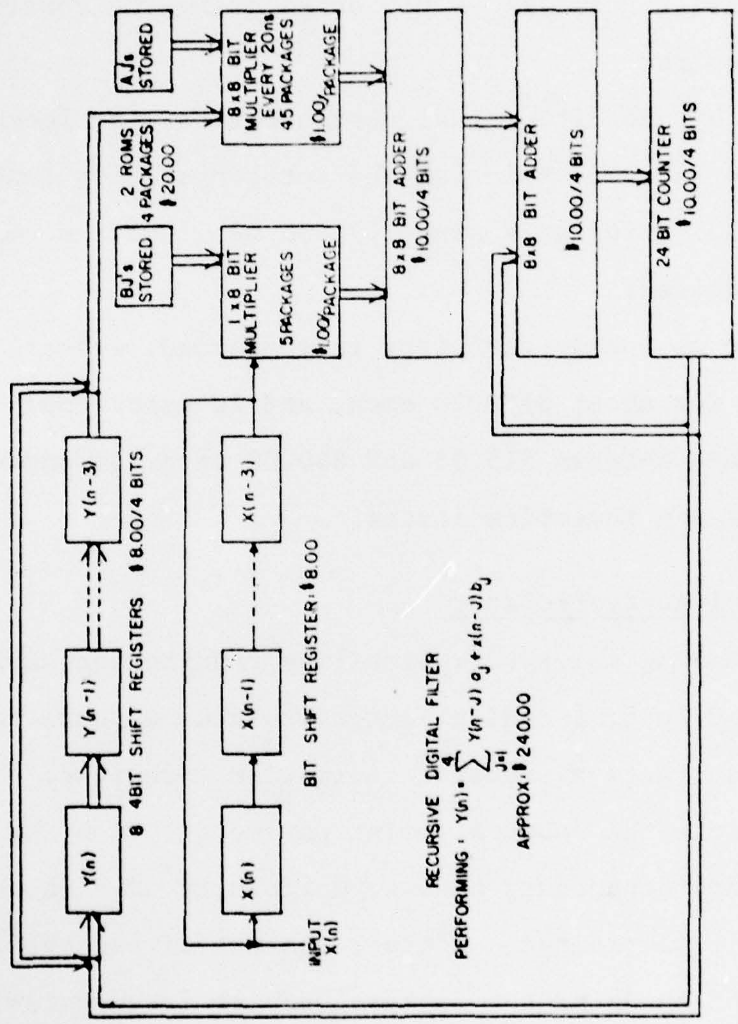

Figure 13. Recursive filter cost estimate

$$y(n) = \sum_{i=1}^{4} y(n-i)a_i + x(n-i)b_i$$

where the input data stream x(n-i) is quantized only to one bit. The basic cost is then approximately $240.00 per spectral point (Figure 13) -- not considering the control circuitry required.

A one by one bit digital autocorrelator is blocked out in Figure 14. One point on the autocorrelation function can then be built for approximately $30.00, less the control circuitry required.

As far as analog circuitry is concerned, crystal filters sell for about $250.00 each, and 20 nanosecond delay lines are between $15.00 and $40.00 each, depending on rise times and insertion losses.

4.4 Digital Autocorrelator

Considering the system stability requirements and the complexity and cost, a digital autocorrelator appears to be the most attractive spectral estimation technique. This choice restricts the spectral point parameters to being relatively interdependent; however, uniformity over the band is then easily maintained. Another feature of the system is the ease of changing the filters' center frequencies. A simple adjustment of the sampling rate will vary $\Delta\tau$ and thus effect a system "fine tuning." This is attractive for locating the peak of the water vapor line.

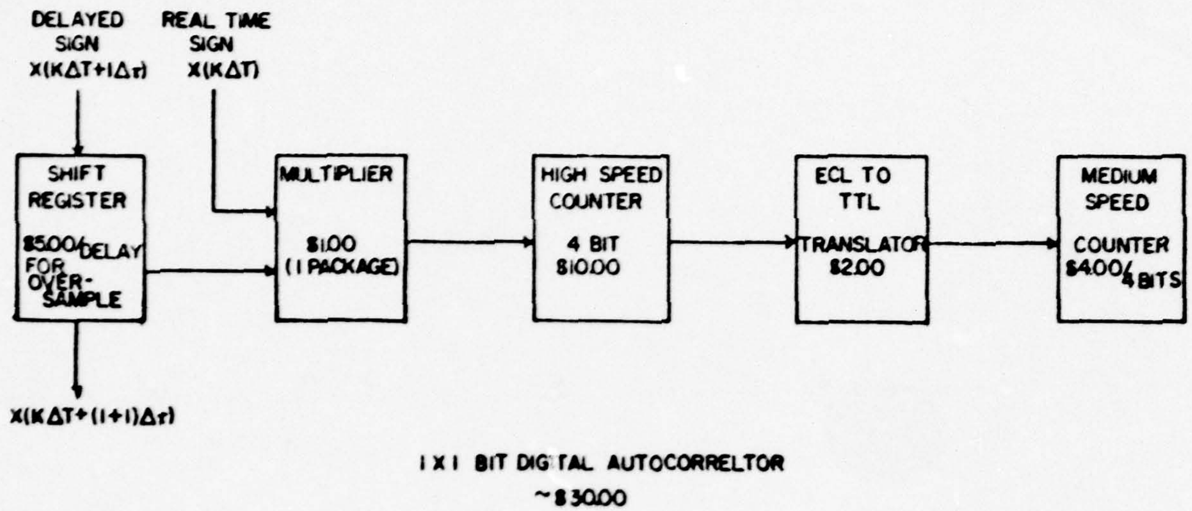

Figure 14. Digital autocorrelator cost estimate

Digital autocorrelation techniques will now be considered in depth and a particular system will be chosen.

CHAPTER V

DIGITAL AUTOCORRELATOR TECHNIQUES

5.1 Available Equipment

The simplest method of digital signal analysis would be a complete software package. The Ionosphere Research Laboratory at The Pennsylvania State University has available a Data General Nova 1200 minicomputer complete with an IBM nine track tape interface. In addition, an IBM 370-168 is available for batch processing at Penn State. The desired system would be to digitize the incoming data and store it on nine track tape via the Nova. Data analysis could then be completed on the IBM 370. However, the 20 MHz IF bandwidth makes a hardware accumulator/buffer necessary, before the Nova could accept the data stream. The hardware accumulator/buffer is to be a high speed digital system performing the autocorrelation function given in Equation (6).

5.2 Sampling Rate

The sampling rate necessary to achieve a 20 MHz band would be 40 MHz, by the sampling theorem. However, the sampling theorem assumes an infinite number of quantization levels. Van Vleck (1943) has shown that the autocorrelation of a grossly quantized Gaussian signal can be corrected to give the actual autocorrelation function.

This means hardware can be simplified. However, the gross quantization causes a decrease in sensitivity. Hagan and Farley (1973) and Cooper (1970) show that an improvement in sensitivity can be attained by over sampling. It will be shown later that sampling at twice the Nyquist rate, 80 MHz, gives nearly maximum improvement in sensitivity. Also, if a frequency "fine tuning" is desired, the sampling rate should be further increased to allow $\Delta\tau$ to vary without decrementing system sensitivity. This concept will be discussed further, but for now it is sufficient to assume that the system should be designed for a sampling rate of 100 MHz.

5.3 Number of Quantization Levels

The next step is to consider the number of quantization levels desired. A large number of bits would decrease the sampling frequency down to around 40 MHz, however, even then a multiplication operation must be accomplished in less than 25 nsec. P. Blankenship and A. Huntoon have done some digital processing work (Rabiner and Gold, 1975) and have accomplished a 9 by 9 bit multiply in 22 nsec using 45 custom 2 bit ECL adders. On the other hand, a number of 1 by 1 bit autocorrelators are presently in operation (Weinreb, 1963; Fell and Little, 1975; Ables, Cooper, Hunt, Moorey, and Brooks, 1974). The 1 bit quantization requires a multiply every 10 nsec; however, a 1 x 1 bit multiplication is simply an "exclusive or" function

and can be accomplished by the ECL III logic series in one nsec. Therefore, a tradeoff exists between hardware complexity and sensitivity. An interesting compromise is a 1 x 2 bit system where the one bit quantization is also the delayed signal. The 1 x 2 bit system still maintains a sign only, or one bit, multiplication. Also, the delayed signal being one bit means only one channel of shift registers is required. The 1 x 2 bit system maintains much of the simplicity offered by the 1 x 1 bit system, however, the sensitivity can approach a maximum of 84% of a multibit correlator (Hagan and Farley, 1973), as opposed to 74% (Hagan, 1972) in the 1 x 1 case. The 1 x 2 bit digital autocorrelator was then accepted as the overall best system for analyzing the water vapor line.

CHAPTER VI

ONE BY TWO BIT CORRELATOR

6.1 Normalized Autocorrelation Function

The 1 x 2 bit autocorrelation estimate, as Van Vleck showed, contains a gross quantization error and therefore must be corrected to provide an equivalent multibit autocorrelation estimate. This correction factor can be arrived at by considering the statistical mean of the normalized autocorrelation function (uncorrected), $r(i\Delta\tau)$. Note that the normalized autocorrelation function is referenced to the zero lag autocorrelation point.

$$r(i\Delta\tau) = \frac{\overline{R(i\Delta\tau)}}{\overline{R(o)}}$$

From Equation (6):

$$r(i\Delta\tau) = \frac{\overline{x(k\Delta t)\ x\ (k\Delta t+i\Delta\tau)}}{\overline{x^2(k\Delta t)}} \qquad (13)$$

Here $x(k\Delta t)$ represents the two bit real time signal and $x(k\Delta t+i\Delta\tau)$, represents the one bit delayed signal. The mean of the signal products can then be represented by the sum of the joint probabilities of each quantization product occurring. The quantization products for 1 x 2 bit quantization scheme are defined in Table 1. Note that

Table 1. One by Two Bit Quantization Products

States:

One bit	$[x(k\Delta t + i\Delta\tau)]$
1	$x > 0$
$\bar{1}$	$x < 0$

Two bit	$[x(k\Delta t)]$
2	$V_o < x < \infty$
1	$0 < x < V_o$
$\bar{1}$	$-V_o < x < 0$
$\bar{2}$	$-\infty < x < -V_o$

Products:

		Two bit			
		2	1	$\bar{1}$	$\bar{2}$
One bit	1	1	n^{-1}	$-n^{-1}$	-1
	$\bar{1}$	-1	$-n^{-1}$	n^{-1}	1

the quantization level, v_o, is normalized to the rms value of the incoming signal. Also the higher products are weighted by n. The proper choice of n will tend to improve sensitivity.

The probability of a particular product occurring is then determined by the joint probability of the corresponding delayed and real time states occurring. Each probability function, P_{dr}, is denoted by the subscripts d and r, indicating the state of the delayed and real time signals, respectively. Equation (13) can then be represented as follows:

$$r(i\Delta\tau)=[(1)(P_{\bar{1}\bar{2}}+P_{12})+(-1)(P_{1\bar{2}}+P_{\bar{1}2})+(n^{-1})(P_{11}+P_{\bar{1}\bar{1}})+(-n^{-1})(P_{1\bar{1}}+P_{\bar{1}1})] \,/\, [(1)(P_{12}+P_{\bar{1}\bar{2}})+(n^{-1})(P_{11}+P_{\bar{1}\bar{1}})]$$

Assuming the input signal is a Gaussian random process with zero mean, symmetry will allow the following reduction.

$$r(i\Delta\tau) = \frac{(P_{12}-P_{\bar{1}2})+n^{-1}(P_{11}-P_{\bar{1}1})}{P_{12}+n^{-1}P_{11}} \tag{14}$$

The joint probability function is then defined by the Bivariate Normal Probability Function (National Bureau of Standards, 1964) where ρ is the normalized correlation.

$$P_{dr} = Q(d)Q(r) + \sum_{N=0}^{\infty} \frac{Z^{(N)}(d)Z^{(N)}(r)}{(N+1)!}\rho^{N+1} \quad (15)$$

Where:

$$Q(x) = \int_x^{\infty} Z(t)dt \quad (16)$$

$$Z(x) = \frac{1}{\sqrt{2\pi}} e^{-x^2/2} \quad (17)$$

$$Z^{(m)}(x) = \frac{d^m}{dx^m} Z(x) \quad (18)$$

Some supporting probability functions are also defined:

$$P(x) = \int_{-\infty}^{x} Z(t)dt \quad (19)$$

$$A(x) = \int_{-x}^{x} Z(t)dt \quad (20)$$

$$P(x)+Q(x) = 1 \quad (21)$$

$$P(-x) = Q(x) \quad (22)$$

$$A(x) = 2P(x)-1 \quad (23)$$

Combining Equations (21) and (23) then provides:

$$Q(x) = \frac{1}{2} - \frac{1}{2} A(x) \quad (24)$$

Where $A(x)$ has been tabulated for various values of x in a variety of handbooks (Dwight, 1947).

The probability functions P_{dr} can now be determined to any accuracy by setting the limit on N in Equation (15). For the probability P_{12}, Equation (15) is used in conjunction with Equations (16) through (24). Here N is set to 4.

$$P_{12} = \frac{1}{4}(1-A(V_o) + \frac{Z(V_o)}{\sqrt{2\pi}}\rho - \frac{[Z(V_o)](V_o^2-1)}{6\sqrt{2\pi}}\rho^3 + \frac{[Z(V_o)](V_o^4-6V_o^3+3)}{40\sqrt{2\pi}}\rho^5 \qquad (25)$$

Obviously as ρ decreases, that is, the signals become less correlated, the higher order terms become less significant.

The probability $P_{\overline{1}2}$ has limits $-\infty$ to 0 for the d parameter. Therefore, Equation (22) can be substituted into Equation (15) giving:

$$P_{\overline{d}r} = P(d)Q(r) + \sum_{N=0}^{\infty} \frac{Z^{(N)}(-d)Z^{(N)}(r)}{(N-1)!}\rho^{N-1} \qquad (26)$$

Then substituting as before gives:

$$P_{\overline{1}2} = \frac{1}{4}[1-A(V_o)] - \frac{Z(V_o)}{\sqrt{2\pi}}\rho + \frac{Z(V_o)(V_o^2-1)}{6\sqrt{2\pi}}\rho^3 - \frac{Z(V_o)(V_o^4-6V_o^3+3)}{40\sqrt{2\pi}}\rho^5 \qquad (27)$$

P_{11} can be found by subtracting P_{12} from the probability defined by both limits d & r going from 0 to ∞. These relationships are then:

$$P_{11} = P_{oo} - P_{12}$$

$$P_{00} = \frac{1}{4} + \frac{1}{2\pi}\rho + \frac{1}{12\pi}\rho^3 + \frac{9}{240\pi}\rho^5$$

therefore:

$$P_{11} = \frac{1}{4}A(V_o) + \left(\frac{1}{2\pi} - \frac{Z(V_o)}{\sqrt{2\pi}}\right)\rho + \left[\frac{1}{2\pi} + \frac{Z(V_o)}{\sqrt{2\pi}}(V_o^2-1)\right]\frac{\rho^3}{6} + \left[\frac{3}{2\pi} - \frac{Z(V_o)}{\sqrt{2\pi}}(V_o^4-6V_o^2+3)\right]\frac{\rho^5}{40} \tag{28}$$

$P_{\bar{1}1}$ is approached similarly:

$$P_{\bar{1}1} = P_{\bar{0}0} - P_{\bar{1}2}$$

$$P_{\bar{0}0} = \frac{1}{4} - \frac{1}{2\pi}\rho - \frac{1}{12\pi}\rho^3 - \frac{9}{240\pi}\rho^5$$

and therefore:

$$P_{\bar{1}1} = \frac{1}{4}A(V_o) - \left(\frac{1}{2\pi} - \frac{Z(V_o)}{\sqrt{2\pi}}\right) - \left[\frac{1}{2\pi} + \frac{Z(V_o)}{\sqrt{2\pi}}(V_o^2-1)\right]\frac{\rho^3}{6} + \left[\frac{3}{2\pi} - \frac{Z(V_o)}{\sqrt{2\pi}}(V_o^4-6V_o^2+3)\right]\frac{\rho^5}{40} \tag{29}$$

The relationship between the normalized uncorrected autocorrelation function, $r(i\Delta\tau)$, and the corrected version, ρ, is found by substituting Equations (25), (27), (28), and (29) into Equation (14). The rather forbidding result can then be solved for ρ by a computer, using iterative methods. However, a simple approximation would be to assume highly uncorrelated signals, as would be the case for Gaussian random process, and that V_o is between zero and approximately one. The ρ^3 and higher order terms then effectively go to zero reducing Equations (25), (27), (28), and (29) as follows:

$$P_{12} = \frac{1}{4}\,[1-A(V_o)]+\frac{Z(V_o)}{\sqrt{2\pi}}\,\rho \tag{30}$$

$$P_{\bar{1}2} = \frac{1}{4}\,[1-A(V_o)]-\frac{Z(V_o)}{\sqrt{2\pi}}\,\rho \tag{31}$$

$$P_{11} = \frac{1}{4}\,A(V_o)+\left(\frac{1}{2}-\frac{Z(V_o)}{\sqrt{2\pi}}\right)\rho \tag{32}$$

$$P_{\bar{1}1} = \frac{1}{4}\,A(V_o)-\left(\frac{1}{2}-\frac{Z(V_o)}{\sqrt{2\pi}}\right)\rho \tag{33}$$

Substituting Equations (30) through (33) into Equation (14) now produces:

$$r(i\Delta\tau) = \frac{2}{\pi}\left[\frac{(1-n^{-1})\frac{Z(V_o)}{\sqrt{2\pi}} + n^{-1}}{A(V_o)n^{-1} - A(V_o) + 1}\right]\rho \tag{34}$$

or an approximation for ρ would then be:

$$\rho(i\Delta\tau) = \frac{\pi}{2}\left[\frac{A(V_o)n^{-1} - A(V_o) + 1}{(1-n^{-1})\frac{Z(V_o)}{\sqrt{2\pi}} + n^{-1}}\right]r(i\Delta\tau) \tag{35}$$

6.2 One by Two Bit Autocorrelator Sensitivity

Cooper (1970) has used this technique for approximating ρ in a 2 x 2 bit autocorrelator. In addition, he went on to find an approximation for the sensitivity (variance) relative to a multibit correlator, and optimized V_o and n to give the highest sensitivity. Hagen and Farley (1973) achieved similar results using Price's theorem to determine ρ. They also calculated outputs and optimum sensitivities for a variety of other quantization schemes, in particular, the 1 x 2 bit system. Their results are given in Equation (36) and show that greatest sensitivity is achieved with V_o equal to 0.95 and n=4.

$$\sigma_\rho^{\ 2} = \frac{\pi^2}{4N}\,\frac{[n^2-(n^2-1)A(V_o)]}{[1+(n-1)Z(V_o)]^2} \tag{36}$$

Where:

N = Number of counts

It is desirable to have n a power of two so that weightings can be easily achieved with a digital counter. With V_o and n optimized, integration times relative to a multibit correlator were found to be 1.78 for sampling at the Nyquist rate, and 1.43 for oversampling at twice the Nyquist rate. A sampling rate higher than twice the Nyquist rate does afford some further increase in sensitivity (Burns and Yao, 1969; Hagan, 1972). However, the slight sensitivity increase does not justify a further increase in bandwidth. It is adequate to realize that sampling faster than two times the sampling rate does not degrade sensitivity.

The relative integration times determined by Hagen and Farley can be converted to relative sensitivities using Equation (1). Since sensitivity is inversely proportional to the square root of integration time, sampling at the Nyquist rate will provide a relative sensitivity of 0.75, and twice the Nyquist rate will increase the sensitivity to .84 of a multibit correlator.

To construct the most sensitive 2 x 1 bit correlator capable of analyzing a 20 MHz bandwidth, a minimum sampling rate of two times the Nyquist rate or 80 MHz is to be used. Then, as previously discussed, to allow some flexibility in the location of the resultant "spectral windows," the sampling rate will be made variable between 80 and 100 MHz. Oversampling can be accomplished by setting $\Delta\tau$ equal to

$2\Delta t$ in Equation (6). This would be equivalent to delaying the signal, $\dot{x}(k\Delta t + i\Delta\tau)$, through two successive Δt clocked flip flops before i is considered incremented. Weighting the higher level products by four is most easily accomplished by considering the higher level products one, and dividing the lower level products by four. An up-down counter will then accumulate the products. A simple block diagram of this system is represented in Figure 12.

CHAPTER VII

SYSTEM HARDWARE

7.1. Logic Families

The fastest Schottky TTL up-down counter listed in the Texas Instruments TTL Data Book will clock at a maximum rate of 40 MHz. This makes the TTL logic series inadequate for the high speed section of the correlator. The Motorola ECL Data Book lists several ECL logic series which feature much faster gate delay times then the TTL families. The ECL III series lists a 1 nsec typical gate delay time as opposed to the 3 nsec delay time offered by the Schottky clamped TTL. Motorola also offers an ECL-10,000 series with gate delay times of 2 nsec. The 10,000 series provides gate rise and fall times intentionally slowed to 2 nsec to help inhibit coupling between adjacent signal lines. The MC 10136 up-down counter lists a 150 MHz maximum clocking rate in the up or down mode. If the up and down modes are used alternately, a maximum clocking rate of 133 MHz is inferred. Also, cascading the counters slows the maximum clocking rate to 95 MHz. An additional feature of the ECL 10,000 series is the variety of MSI and LSI functions. The readily available array of complex functions is comparable to the Schottky TTL series. Thus, the ECL 10,000 series appears adequate to provide the necessary high speed logic. The higher cost associated

with ECL ($10.50 for a four bit binary up-down counter) will then restrict ECL to only the high speed section. Subsequent lower speed sections will then be built from the less expensive TTL families.

The ECL 10,000 series consists of open emitter follower output stages. Therefore, with the proper pull down resistor, each logic gate can become a line driver or each gate can drive low impedance transmission lines, down to an impedance of 50 ohms. At switching times of 100 MHz, transmission line effects become important and, thus, should be considered in circuit board layouts.

First, however, the power supply voltage should be considered. According to Motorola's ECL data book, a supply voltage of -5.2 volts will provide best noise immunity. The resulting logic levels are then -0.9 volts for a logic high or "1" and -1.75 volts for a logic low or "0." The resulting logic level transition voltage is -1.29 volts.

7.2 Crosstalk

Crosstalk should be considered at these switching speeds and is easily handled by using a method described in an article by Robert Saeger of Signetics Corporation (1974). Jaeger describes the relationship between the sending and receiving line in the form of pulse widths and amplitudes induced onto the receiving line. For the

purposes of the system here, pulse widths are fairly unimportant, provided the induced pulse amplitudes are small. Crosstalk is broken down into a forward going pulse relative to the sending line and backward pulse. The forward and backward crosstalk amplitudes were determined by Jaeger to be:

$$V_f = \frac{K_f V_s}{tr} \ell \tag{37}$$

$$V_b = K_b V_s \tag{38}$$

Where:

V_f = Amplitude of forward pulse

V_s = Amplitude of sending pulse

V_b = Amplitude of backward pulse

ℓ = Length of parallel sending and receiving lines in feet

t_r = Sending pulse rise time in n sec

K_f = Forward crosstalk coefficient

K_b = Backward crosstalk coefficient

The coefficients K_f and K_b are dependent on the spacing between sending and receiving lines and are provided in chart form by Jaeger and repeated here in Figure 15a and b.

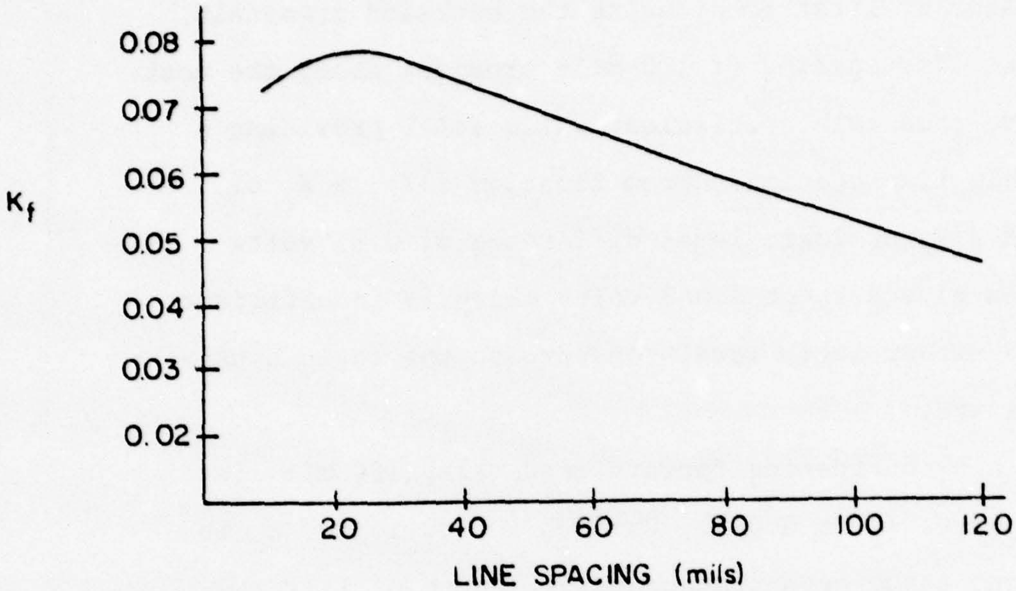

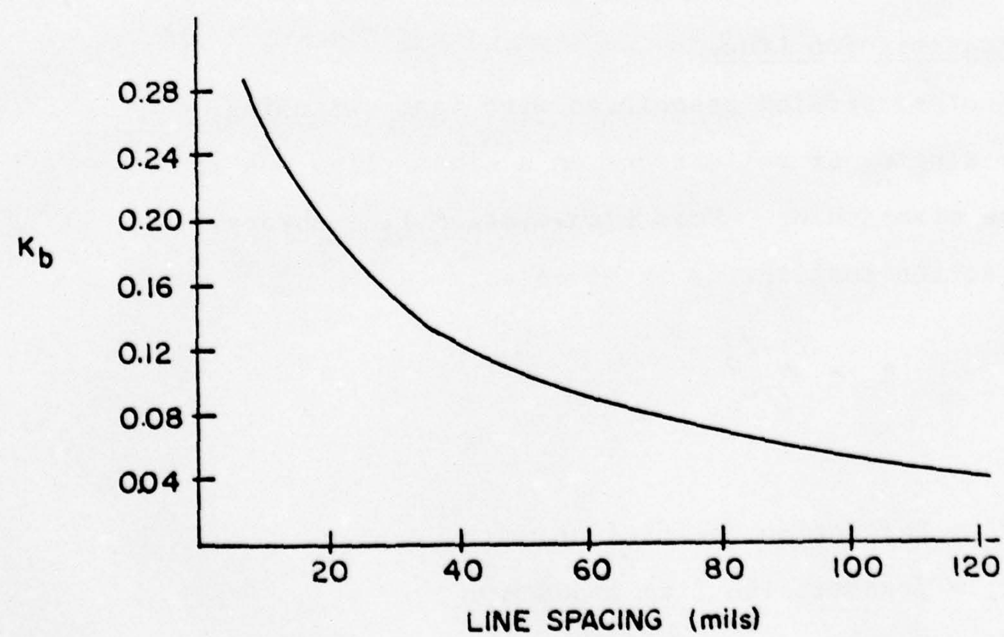

Figure 15. a) K_f; b) K_b (both after Jaeger, 1974)

Now, by first considering the backward crosstalk, a minimum line spacing of 100 mils provides about the most effective crosstalk coefficient while still providing a reasonable line spacing. From Equation (37), a K_b of 0.05 and a V_s or logic level difference of 0.85 volts will then give a V_b of 0.043 volts which is insufficient to cause either logic level to approach the logic cross-over voltage.

Then considering forward crosstalk, 100 mil line spacing gives K_f as 0.055. For ECL 10,000 logic, t_r is 2 nsec and assuming a crosscoupling length of 1 ft, V_f becomes 0.023 volts. Forward crosstalk is therefore less of a problem then backward crosstalk.

7.3 Transmission Lines

Another problem associated with fast switching lines is ringing or reflections on a signal line due to impedance mismatching. From transmission line theory, the reflection coefficient is given as:

$$K_R = \frac{Z_L - Z_o}{Z_L + Z_o} \tag{39}$$

Where:

K_R = Reflection coefficient

Z_o = Transmission line impedance

Z_L = Termination or load impedance

The easiest method to inhibit ringing then is to make $Z_L = Z_o$. Thus, the value of the pull down resistors for each logic output is dependent on the signal line impedance. The value of Z_o can be estimated from a microstrip representation of the circuit board. Using a glass-epoxy circuit board of width 0.0625" and permittivity of 4.6, the impedance can be determined from Figure 16. The impedance is depedent on signal line width, assuming the line thickness is small compared to width. A typical line thickness will be approximately 1.5 mils, whereas the smallest easily etchable widths will be 10 to 20 mils.

Since the ECL 10,000 series was intended to drive low impedance loads, a wide line width is desired. The widest pratical line width for connections to DIP circuit packages is 50 mils. If a ground plane could be managed, a Z_o of 75 ohms would be maintained. However, two sided circuit boards were required in the circuit layouts, therefore only partial ground grid patterns were constructed on both sides of the board. The resulting effect would be to increase the average line impedance and lower the uniformity along the line. This lack of carefully controlled line impedance may seem crude, however, Jaeger suggests that the ECL 10,000 series will work even if wire-wrapped connections are used.

The actual terminations, or pull down resistors were found experimentally. A Tektronics 475 oscilloscope was the best oscilloscope available, however, the bandwidth

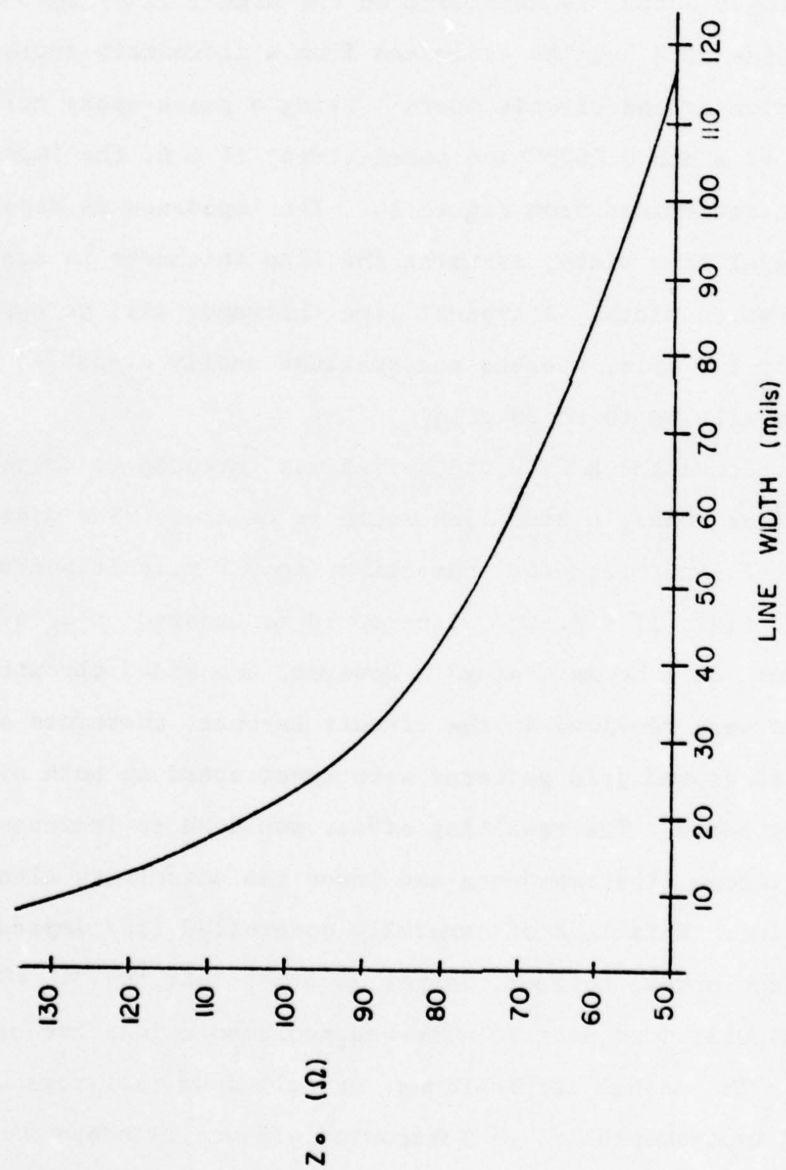

Figure 16. Microstrip impedance (after Jaeger, 1974)

was only 200 MHz. This made the detection of ringing on a 100 MHz square wave impossible. Thus, the terminations were made 220 Ω, which gave the highest amplitude signal at the receiving ends of a majority of transmission lines.

One other circuitry problem is the connections between circuit boards. Because of the lack of good ground planes, chip to chip connections between boards were made for high speed signals using twisted pair lines. Number 24 wire with approximately 18 turns per foot was used.

The following chapters will describe the actual circuitry used.

CHAPTER VIII

CIRCUITRY

8.1 Quantizer

The quantizer was constructed on the timing generation board (TG) utilizing two Motorola MC 1650 comparators. These comparators have a compare time of 3.5 nsec and include D flip-flop outputs. Although each ECL 10,000 series output is capable of driving up to 90 gates, rise time does increase with fanout. Thus, fanout was kept to a maximum of 4, and the sytem was designed to accommodate 16 autocorrelation points. This circuitry is shown in Figure 17.

Note here that V_o and $-V_o$ were set to +.5 v. and -.5 v., respectively. This indicates an analog signal of 475 mv. rms is required to provide the system sensitivity previously discussed. The accuracy of V_o will affect system sensitivity according to Equation (36). From the work of Hagan and Farley (1973), Equation (36) will result in an integration time relative to a multibit correlator and is plotted in Figure 18 verses V_o superimposed in the relative sensitivity as derived from Equation (1). Obviously the value of V_o is not critical. A 10% change in the optimum V_o will result in only a 0.13% degradation in sensitivity.

8.2 High Speed Accumulator

The high speed section (HS) runs synchronously from a 100 MHz master clock. Figure 19 shows the delay

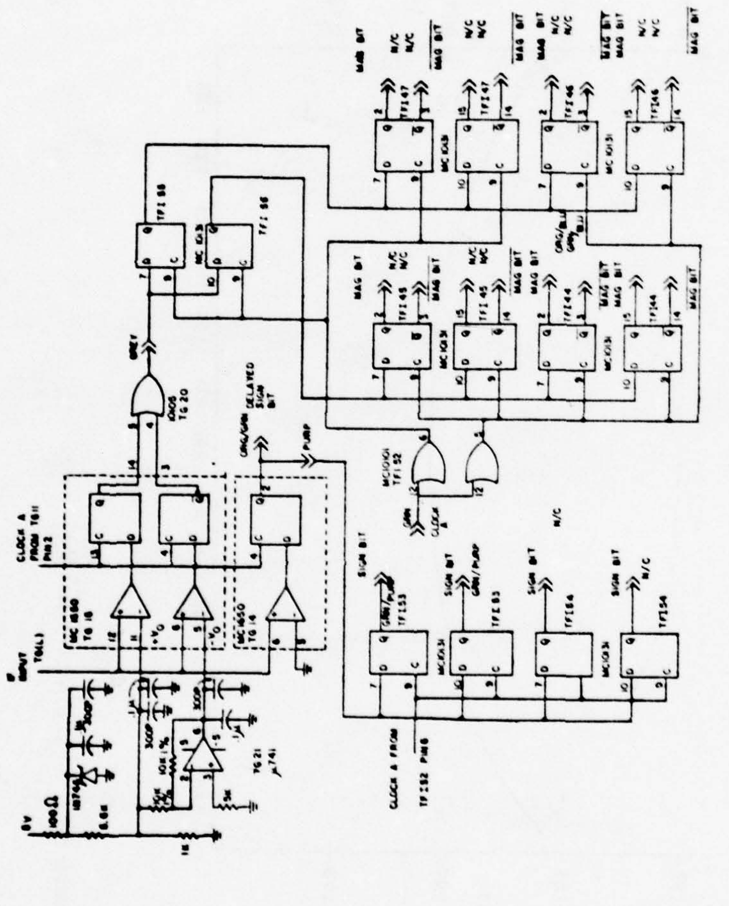

Figure 17. Quantizer

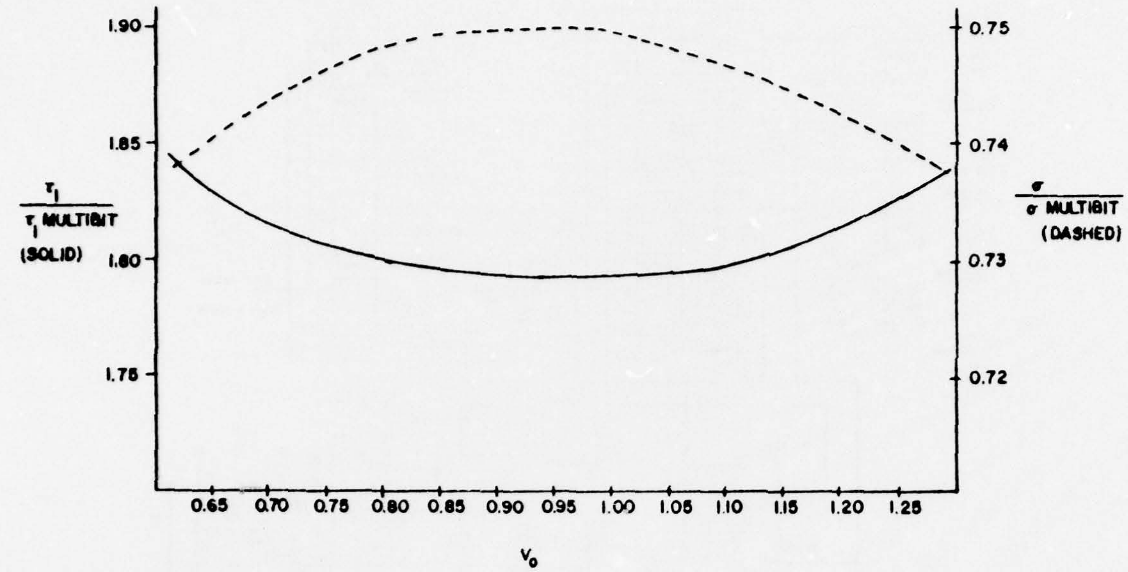

Figure 18. τ_I and σ vs. V_o

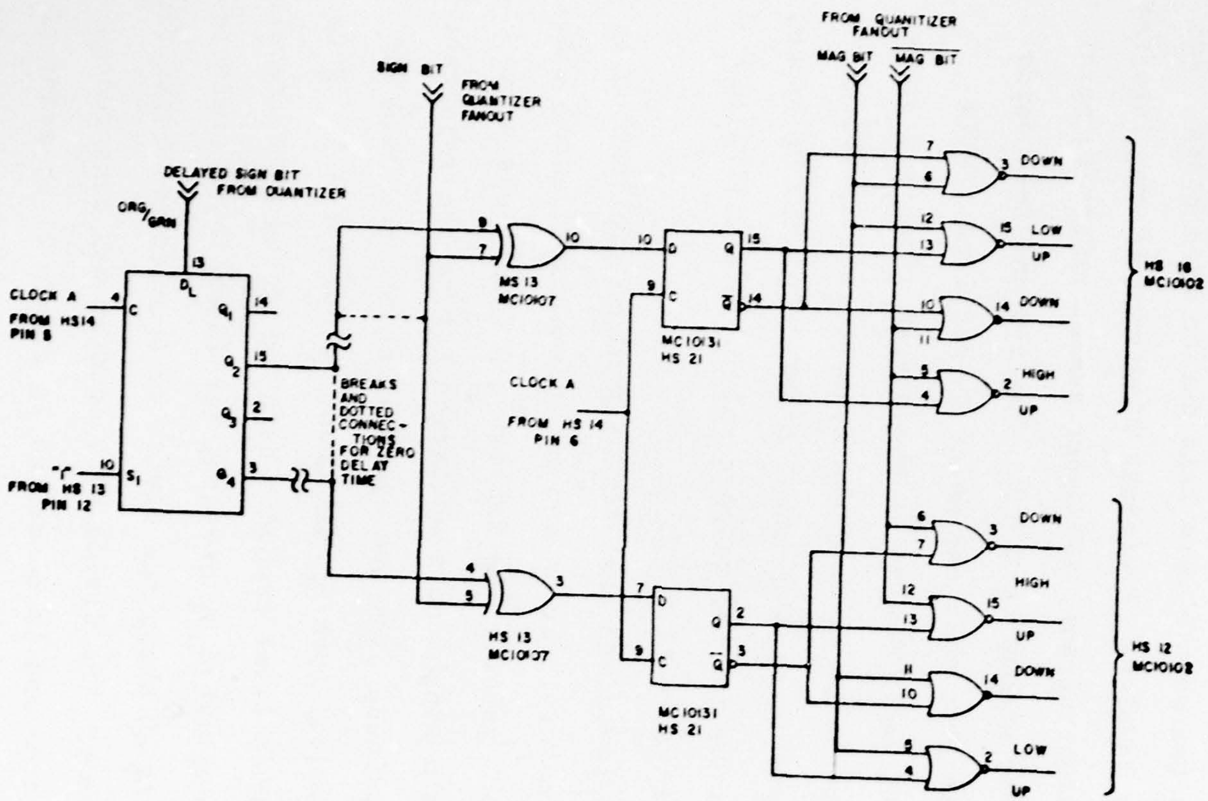

Figure 19. Delay line and multiplier

line and multiplier. The delay line, an MC 10141 shift register, will allow two autocorrelation points if oversampling is used. Thus, in Equation (6), $\Delta\tau = 2\Delta t = 20$ nsec, and therefore two points were laid out on each board. Relating to the labeling of circuit diagrams, if two integrated circuit number appear, the upper number refers to point i and the lower number to i + 1. The i=0 and i=1 boards are special in that only one delay is required. This special wiring is indicated by the dotted lines and break marks. If operation at only the Nyquist rate is preferred, the connections to pins 15 and 3 on MC 10141 can be broken and jumped to 14 and 15, respectively. This will allow operation with $\Delta\tau = \Delta t$.

The delayed and real time signal multiplication is only a sign multiplication and is accomplished using 10107 "exclusive or" gates. The following D flip-flops serve only to retain synchronous operation before the resultant sign and magnitude bits are combined to produce high and low level counts, both up and down, as per Table 1. Note that the higher level products being weighted by n (recall n=4) is accomplished by dividing the lower level products by n. Figure 20 shows the divide by 4 circuitry built from J/K flip-flops. The divide by 4 counter was constructed as a Mealy machine and is described in Figure 21 by means of the flow diagram and coded state table. The outputs were then or'ed with the high level counts and the result

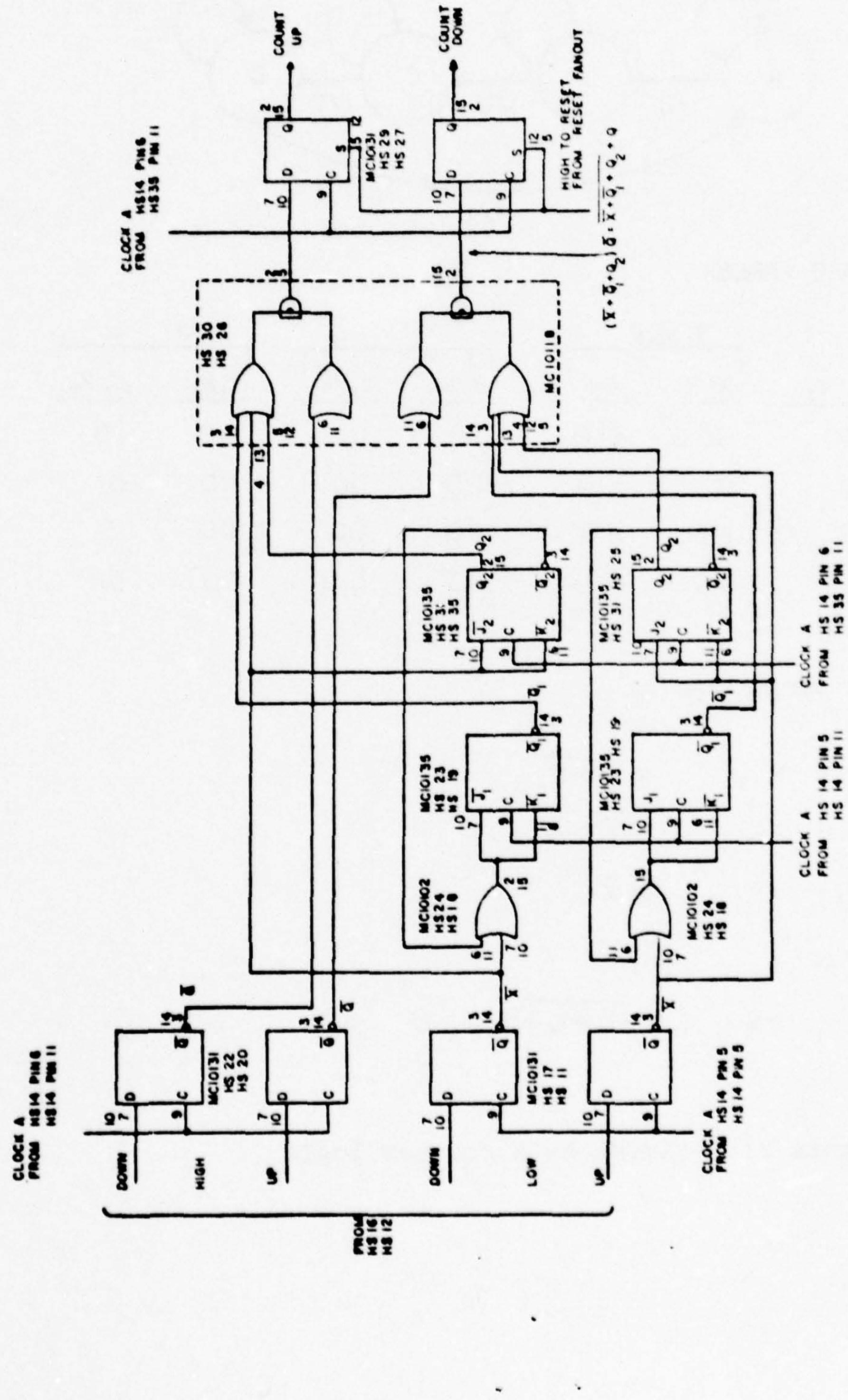

Figure 20. Weighting counters

FLOW DIAGRAM

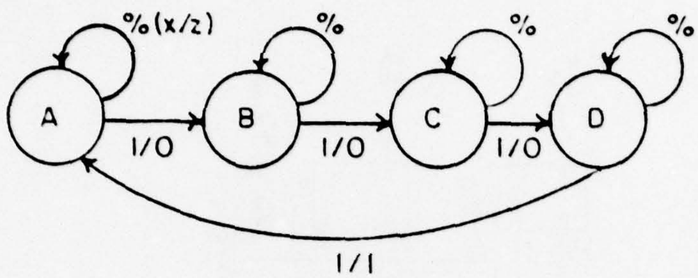

CODED STATE TABLE:

		$Y_1 Y_2, Z$		X=0		X=1	
	$Y_1 Y_2$	X=0	X=1	$J_1 K_1$	$J_2 K_2$	$J_1 K_1$	$J_2 K_2$
A	00	00,0	01,0	0D	0D	0D	1D
B	01	01,0	10,0	0D	D0	1D	D1
C	10	10,0	11,0	D0	0D	D0	1D
D	11	11,0	00,1	D0	D0	D0	D1

RESULTANT FUNCTIONS:

$J_1 = XY_2 \quad \therefore \quad J_1 = \overline{X} + \overline{Q_2}$

$K_1 = XY_2 \quad \therefore \quad \overline{K_1} = \overline{X} + \overline{Q_2}$

$J_2 = X \quad \therefore \quad \overline{J_2} = \overline{X}$

$K_2 = X \quad \therefore \quad \overline{K_2} = \overline{X}$

$Z = Y\overline{Y}X \quad \therefore \quad Z = \overline{\overline{Q} + Q + \overline{X}}$

Figure 21. Divide by 4 counter logic

manipulated to fit an MC 10118 bilevel gate. The counts are then accumulated in an MC 10136 binary up-down counter shown in Figure 22.

Because of the high expense of ECL counters, a transfer was made to TTL at this point. The MC 10136 is operated as a divide by 16 counter carrying only one bit to the lower speed accumulators. At the start of each 16 count cycle, the counter is preloaded to 8 and then tested for a positive or negative pass through zero. A positive or negative count greater than eight is then carried to the TTL counters, facilitating a rounding operation. The reset pulse which then reloads the counter to eight is entered via the output flip-flops shown in Figure 20. The zero detection, denoted x, had to be derived from the counter outputs since the carry bit used in cascading has too great a propagation delay time. The present count's sign, denoted s, was easily derived from the up-down inputs with a single J/K flip-flop. The logic for determining a TTL count and its corresponding sign is shown in Figure 23 in the form of a flow diagram and coded state table.

The effect of using what amounts to a second quantization scheme here can intuitively contribute to a further decline in sensitivity. In actuality, however, the decline in sensitivity can be made negligible if the incoming signal is somewhat correlated and the number of samples is very large. Appendix A provides further analysis of this type of rounding error.

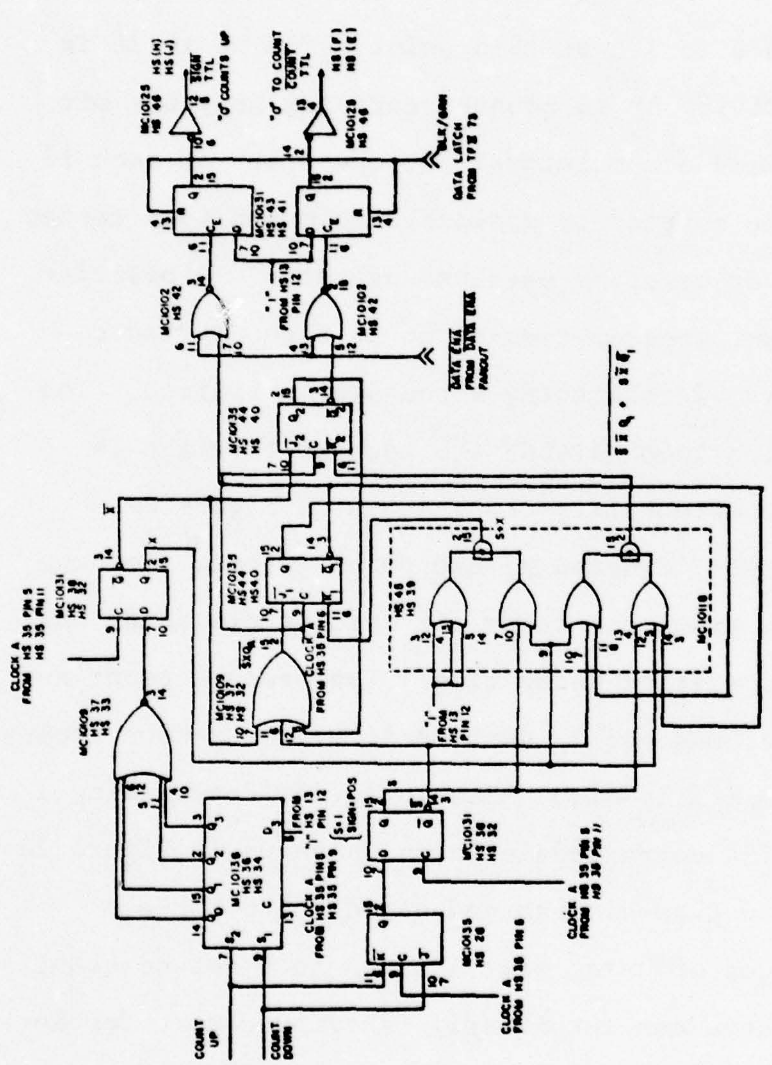

Figure 22. High speed counter

FLOW DIAGRAM:

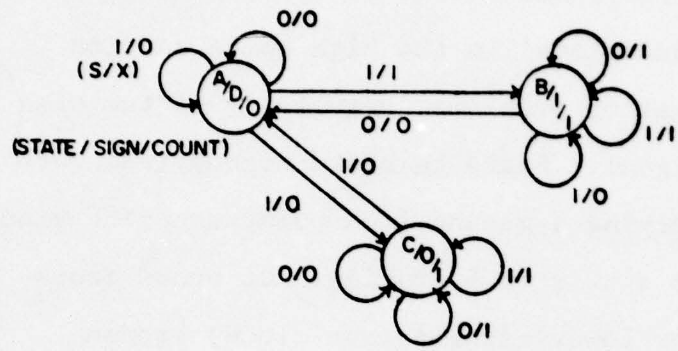

CODED STATE TABLE:

		OUTPUT	$Y_1\ Y_2$				$J_1\ K_1$ / $J_2\ K_2$			
	$Y_1\ Y_2$	SIGN COUNT	SX 00	01	11	10	SX 00	01	11	10
A	0 0	D 0	01	01	11	00	0D 0D	0D 1D	1D 1D	0D 0D
B	1 1	1 1	00	11	11	11	D1 D1	D0 D0	D0 D0	D0 D0
C	0 1	0 1	01	01	01	00	0D D0	0D D0	0D 0D	0D D1

RESULTANT FUNCTIONS:

$J_1 = SX\overline{Y}_2 \quad \therefore \quad \overline{J}_1 = \overline{SX\overline{Q}_2}$

$K_1 = \overline{S}\overline{X} \quad \therefore \quad \overline{K}_1 = S+X$

$J_2 = X \quad \therefore \quad \overline{J}_2 = \overline{X}$

$K_2 = \overline{X}\overline{S}Y_1 + S\overline{X}\overline{Y}_1 \quad \therefore \quad K_2 = \overline{\overline{S}\overline{X}Q_1 + S\overline{X}\overline{Q}_1}$

$SIGN = Y_1 \quad \therefore \quad SIGN = Q_1$

$COUNT = Y_2 \quad\quad COUNT = Q_2$

Figure 23. High speed counter logic

8.3 Signal Propagation

The use of two sided boards as opposed to three sided (center ground plane) in the high speed section caused some propagation problems, especially of the high frequency clock signal. Board to board connections were done simply by carrying a ground from point to point along with the signal in a twisted pair line. On board propagation of 50 MHz or lower signals (non-clock) proved not to be a problem when terminated at a single destination with 220 Ω. The 100 MHz clock signal however, proved more difficult in some instances which were rectified as follows:

1. Occasionally reflections at the source only will be a problem, thus a source termination of 220 Ω is effective.

2. When reflections at both source and destination are a problem or crosstalk signals appear, a destination terminated with 220 Ω and the source terminated with a small capacitance (10-20 pf) is effective.

3. For badly distorted signals, a twisted pair line directly connecting source to destination and terminating the destination in 200 Ω transmits the signal.

4. If long board to board connections cause excessive attenuation, a differential twisted pair can be run using ECL chips 10115 and 10101.

When many high speed boards are used, approximately equal length lines are required to transmit the various signals to each board. Proper operation of each board can be determined by placing a short pulse (10 nsec) on the analog input then measuring the time delay between the real time and delayed sign bits. This measurement can be made at HS 13 pin 7 and HS 13 pin 9 or their equivalents. The delayed pulse should follow the real time pulse by the proper number of delays. Adjustment of the delayed time pulse can be made by "phasing" (delaying) the clock signal at that particular board using one or more gates. These gates are provided on HS 14a. The real time signal should not be delayed as this signal will be in phase with the magnitude, reset, and enabling pulses.

8.4 Medium and Low Speed Accumulators

Four medium speed accumulators with twelve bit tri-state latches are included on one printed circuit board. Figure 24 shows the circuitry with the package and pin numbers shown in quadruplicate. The top number refers to channel i and then in descending order to channel i + 3 as referenced to Equation (6). These 74LS191 up-down counters accumulate the counts produced by the high speed section and are synchronously clocked by the 100 MHz master divided by 18. Although only 16 counts were made in the high speed section, two counts were required to allow for

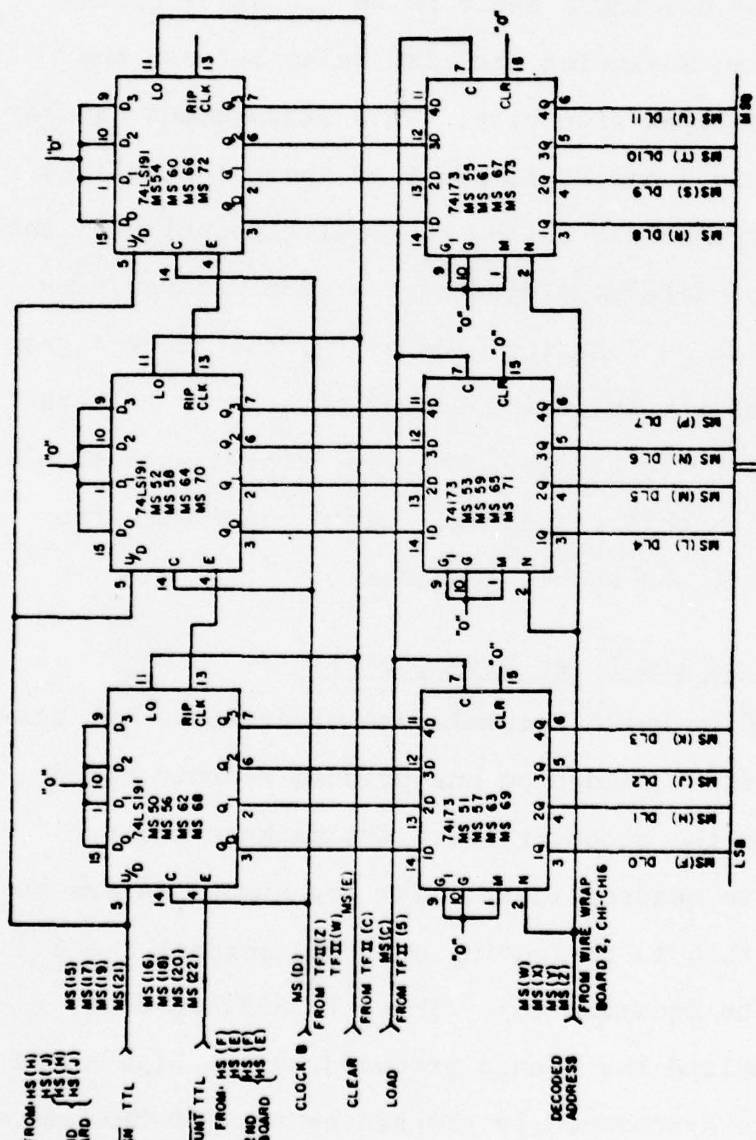

Figure 24. Medium speed accumulator

the reset pulse, thus forcing the medium speed counters to be clocked at 1/18 speed. This will also decrease sensitivity by $\sqrt{1/9}$ since 1/9 of the samples are not used. The 12 bit word accumulated is in two's compliment form, the most significant bit being a sign bit. Therefore, the counters are operated as divide by 2, loading the contents into three 74173, four bit latches every 3.6864 nsec. The latch outputs are then all bussed together to form the 12 bit data link (DLϕ to DL11).

The low speed accumulator is built on board one of two wire wrap boards. This accumulator uses eight Intel 2111A-4 RAM's producing 256 32-bit words. A 256 deep RAM allows for an eventual system expansion to 256 points. With the RAM cycle time of only 450 nsec, this not only allows all RAM words to be accessed but also allows approximately 13.9 μs to manipulate each word before the medium speed latches are reloaded. The 32-bit word width, accessed via a 74LS257A, 2 to 1 multiplexor allows most efficient access from 16 or 8 bit computer systems. Also, using a two's complement word configuration, the 32-bits will accumulate a maximum of 1048576, 12 bit two's complement words. In accumulation time, this amounts to about 64 minutes. Thus, interfacing to most computer systems should not be a difficult procedure.

The RAM word is added to the incoming 12-bit word as shown in Figure 25. The 12-bit word can be added or subtracted from the running sum as desired via the invert control. A low on this line adds while a high subtracts. The invert control is also connected to the least significant carry input on the 32-bit full adder. This facilitates adding one after a complement to provide a two's complement negation. Thus, the RAM word is read, added to the 12-bit data bus, and the result stored in the 32-bit data bus. The 32-bit 2 to 1 multiplexor then allows the sum to be written back into RAM, or allows the RAM to be cleared by reloading with the present 12-bit word.

The computer interface logic, also shown in Figure 25, is built on board two of the wire-wrap set. Six 74365 tri-state drivers form a bus receiver which isolates the computer action from the continuous correlator operation. Before each word in the low speed accumulator (RAM), discussed above, is reloaded, the accumulator read phase writes the existing sum into a second 32 x 256 buffer RAM. The select pulse controls this operation and allows the accumulator RAM to be loaded into the buffer RAM at least once every 64 minutes, as previously discussed. Removing the select pulse then turns control of the buffer RAM over to the computer through two sets of multiplexors. The present system is designed to be accessed from a 16 bit Nova 1200 built by Data General Corporation. Using the

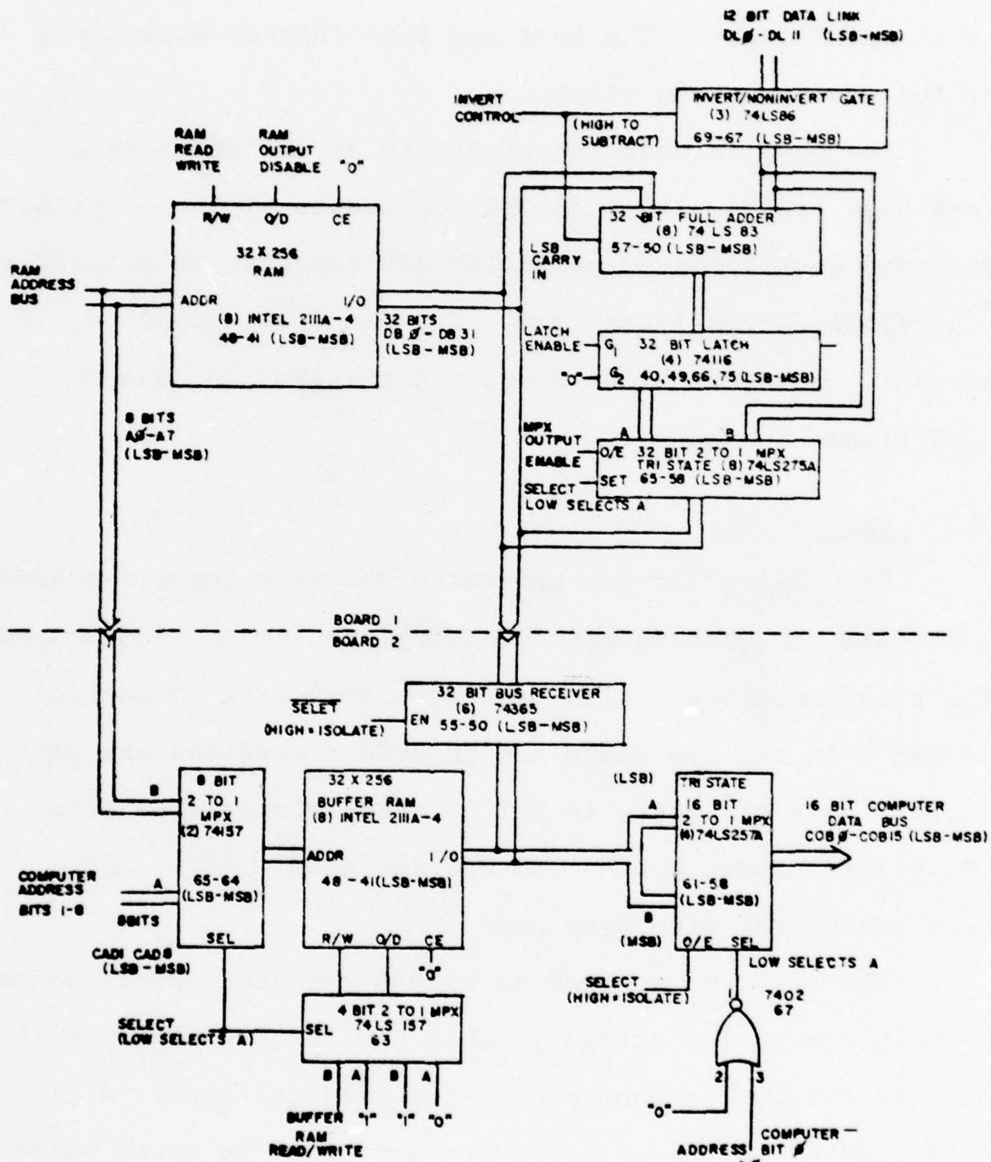

Figure 25. Low speed accumulator and interface

Nova's least significant address bit as a selector, the upper and lower 16 bits are accessed alternately through a 2 to 1 multiplexor. The Nova can then further accumulate for the experiment duration.

The Nova is also interfaced to an IBM compatible 9 track tape drive. Thus, at the conclusion of the experiment, data can be transferred to an IBM 370 computer in a totally or partially accumulated form. The final accumulation, if necessary, along with the Fourier Transform can then be accomplished on the 370.

8.5 Timing

The timing section generates the wave forms required to execute the loading and resetting used in the medium and high speed sections. Also, the waveforms used to control the RAM's in the low speed and interface sections are generated. This circuitry is built on the timing generation (TG) board, fanout boards one and two (TFI, TFII), and board two of the wire wrap pair.

The reset pulse used to reload the high speed counter, shown in Figure 22, actually takes two 10 nsec clock periods. Thus, 16 pulses are counted and two used to reset. A divide by 18 counter is then required to generate the reset pulse as shown in Figures 26a and 26b. Here, the 10136 counter is forced to stop counting for two pulses via the associated flip-flops and gates. The flow diagram and coded state table describing this circuitry is shown in Figure 27.

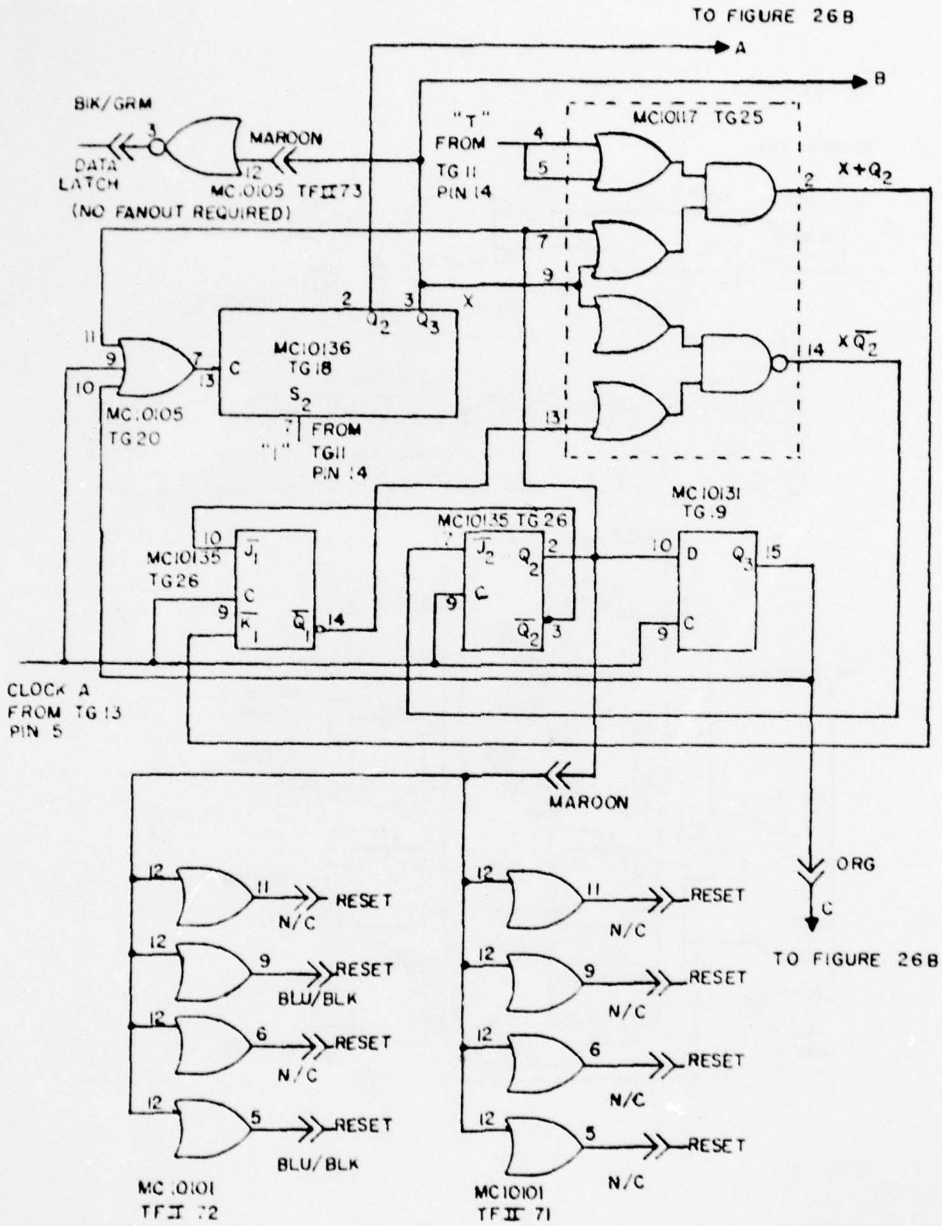

Figure 26a. Timing generation

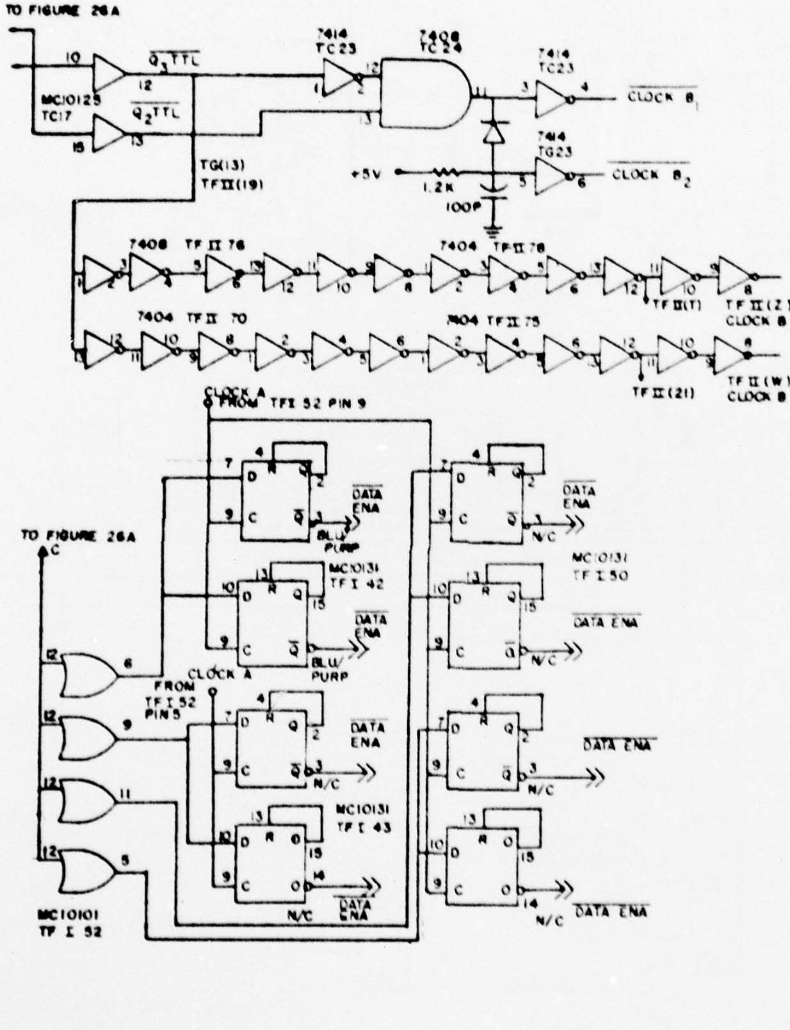

Figure 26b. Timing generation

FLOW DIAGRAM:

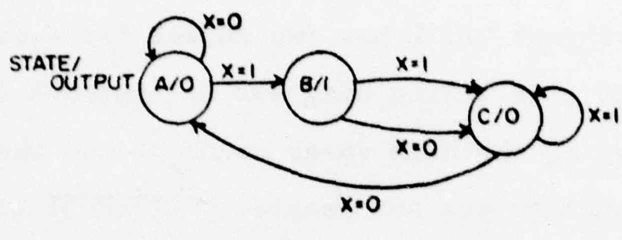

CODED STATE TABLE:

		Y_1Y_2			X=0		X=1	
	Y_1Y_2	X=0	X=1	OUTPUT	J_1K_1	J_2K_2	J_1K_1	J_2K_2
A	00	00	01	0	0D	0D	0D	0D
B	01	10	10	1	1D	D1	1D	D1
C	10	00	10	0	D1	0D	D0	0D.

RESULTANT FUNCTIONS:

$J_1 = Y_2 \quad \therefore \bar{J}_1 = \bar{Q}_2$

$K_1 = X\bar{Y}_2 \quad \therefore \bar{K}_1 = X + Q_2$

$J_2 = X\bar{Y}_1 \quad \therefore \bar{J}_2 = \overline{X\bar{Q}_1}$

$K_2 = 1 \quad \therefore \bar{K}_2 = 0$

$\text{OUTPUT} = Y_2 \quad \therefore \text{OUTPUT} = Q_2$

Figure 27. Timing generation logic

The two most significant counter bits are then level shifted to TTL. Q2TTL then clocks the medium speed counters. Although Q2TTL has two pulses for every 18 high speed counts (see timing diagrams in Appendix B), one pulse occurs during the high speed count period when the medium speed counters are not enabled. $\overline{\text{Clock B1}}$ is generated from Q2TTL and Q3TTL (see Appendix B).

Clearing the medium speed counters and setting the 12 bit latches must occur before the medium speed counters overrun the sign bit. This allows a maximum of 2047 counts before the low going load pulse loads the present count into the 74173 latches. The load occurs on the load pulse rising edge which also triggers the low going clear pulse. The clear pulse low level then clears the 74LS191 counters. Figure 28 shows the divide by 2047 counter used to produce the clear and load pulses. $\overline{\text{Clock B1}}$ and the stretched version, $\overline{\text{Clock B2}}$, are derived from Q3TTL and Q2TTL to clock the divide by 2047 counter. $\overline{\text{Clock B1}}$ had to be stretched in order to accommodate the the short ripple output of TG22. Note at this stage an external reset line is provided. A low on this line will allow the high speed section to fill with new information when the analog source is switched to a reference. The delay involved to reload the high speed section will be less than 300 nsec for 16 points.

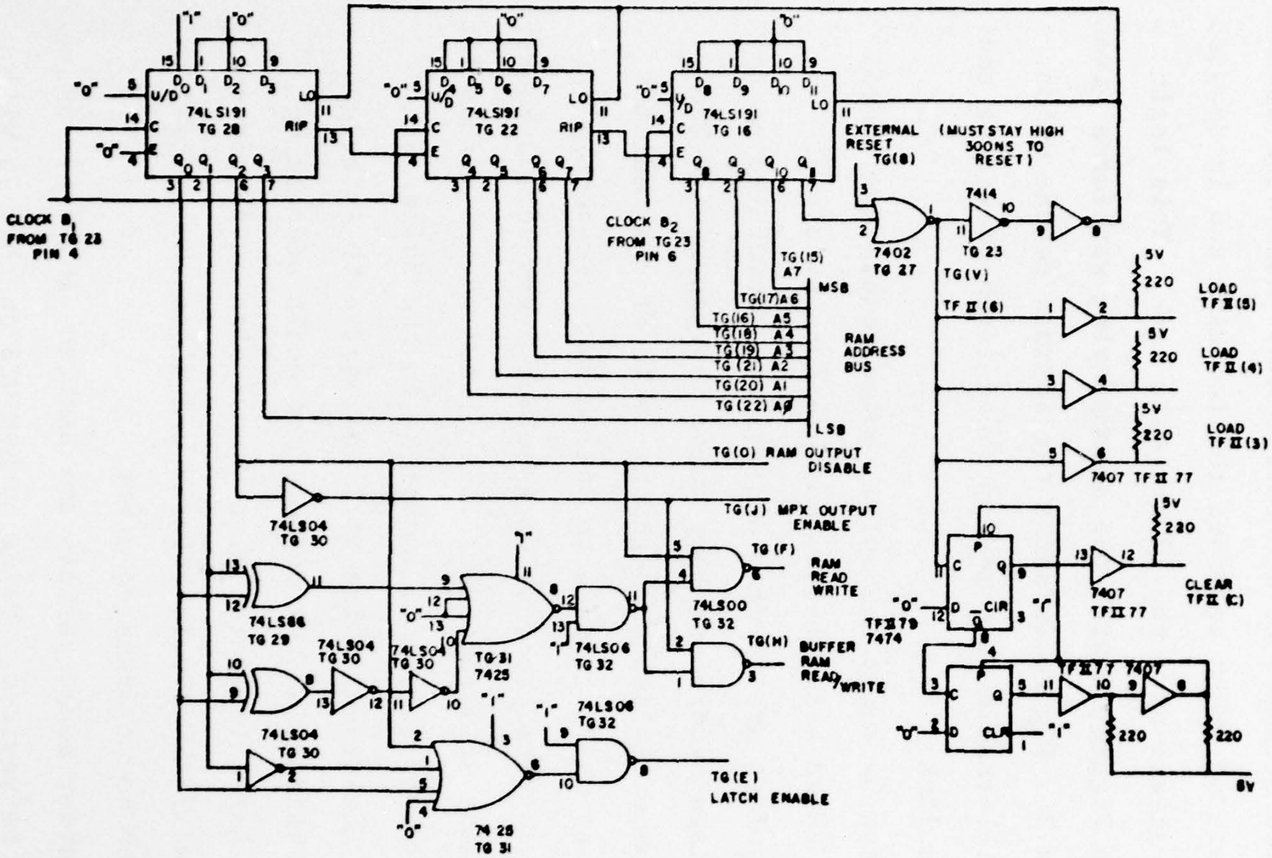

Figure 28. Low speed timing

In addition to the clear and load pulses, the divide by 2047 counter generates the waveforms used to control the low speed accumulator and buffer RAM. Also, the address bus is generated which accesses the two RAMs and is decoded to provide access onto the 12 bit data link. This logic is shown in Figure 28 with the accompanying waveforms given in Appendix B. Figure 29 shows the address decode which, in turn, will enable each medium speed latch to access the 12 bit data link.

Figure 30 shows the select pulse generation, used in the low speed accumulator and interface sections. Here load pulses are counted and can be accumulated up to 1048575 pulses before a select pulse is generated. The select pulse will last through one cycle of the medium speed counter which amounts to 368.38 μsec. Presently the system is wired to provide a select every 262143 counts or about every 96.5 seconds. This allows over a minute for the Nova 1200 to access 16 locations in the buffer RAM. The end of the select pulse will then serve to interrupt the Nova, instructing the computer to begin addressing the buffer RAM. In addition, a manual high on the start line here will clear this counter and allow the initial 1 1/2 minute count frame to start.

If other count periods are desired, chips 67, 69, and 76 can be rewired. Using output Q16 on chip 76 will provide a cycle time of 24 seconds, Q17: 48 seconds,

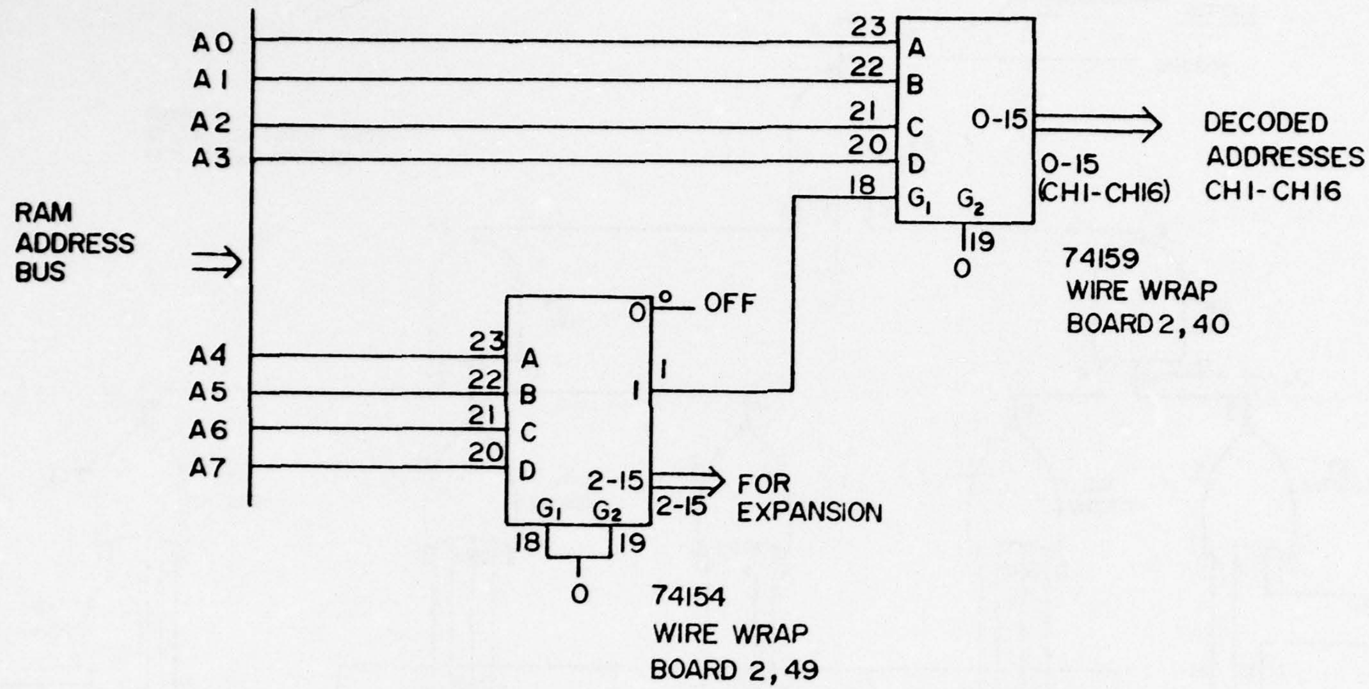

Figure 29. RAM address decoding

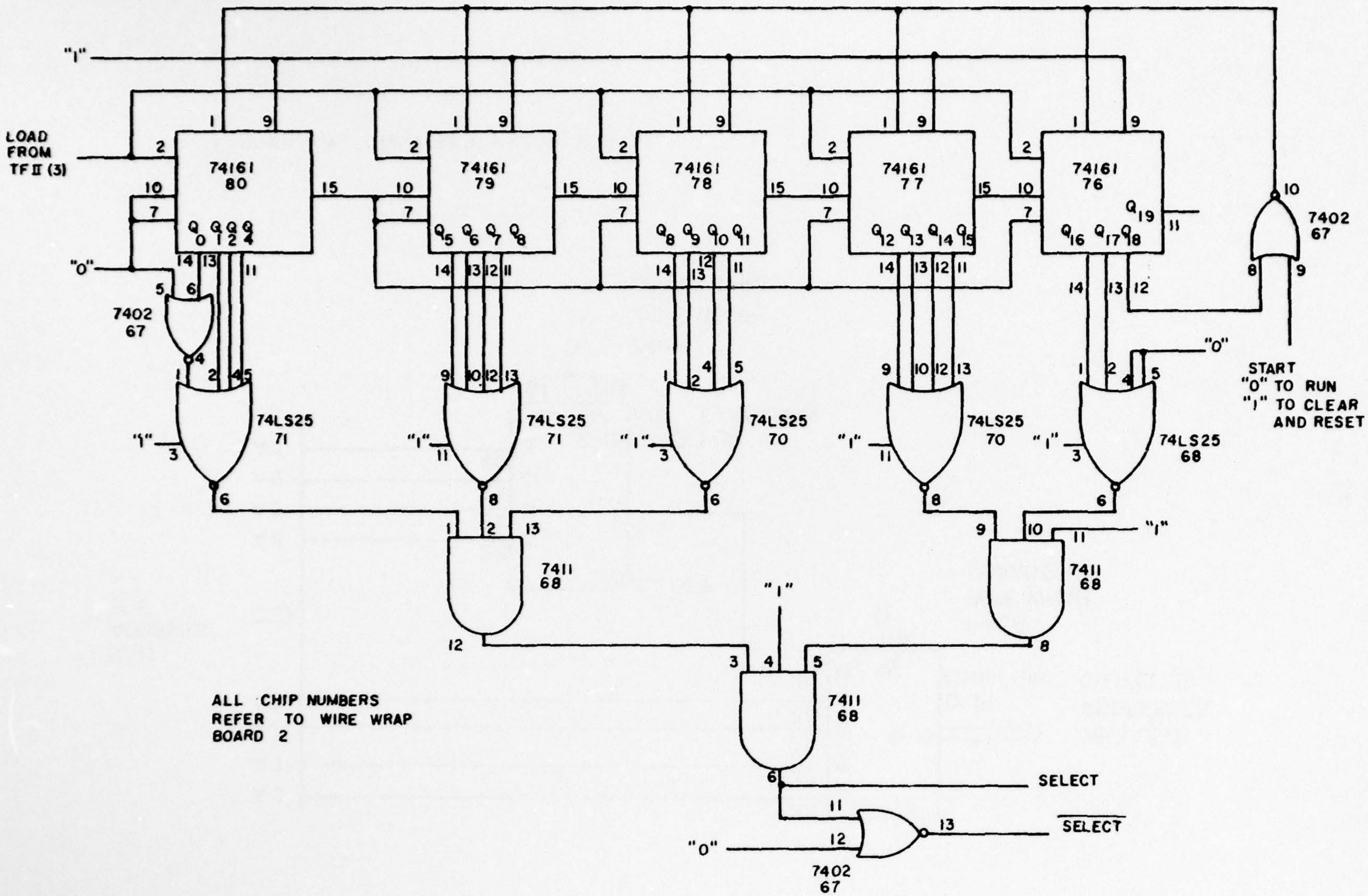

Figure 30. Cycle timing

Q18: 96.5 seconds, Q19: 193 seconds, and using no outputs, that is, allowing the counters to completely cycle through zero, will provide 386 seconds. Appendix B gives the timing diagrams describing the entire system.

CHAPTER IX
SYSTEM OPERATION

9.1 Initialization

The initial start up of the correlator is controlled by the low speed logic, in particular, the select pulse generator. After turn on, the start line is manually held high until the measurement is to commence. Thereafter, one load pulse will be counted before the first select pulse provides an interrupt for the Nova, and the buffer RAM is loaded into Nova core. Since there is no way of determining the initial medium speed counter status, this first data set is ignored. The following full cycle will then provide the first good data set.

9.2 Reference Switching

The next phase is to view a reference source, achieved by switching the frequency of the radiometer local oscillator. This will provide a background noise signal equivalent in temperature (see Figure 1) and variance to the signal frequency band. Thus, viewing this background reference for an equal time and subtracting this information from the signal information, will also subtract out any signal or receiver DC bias. The result will be a relative measurement with only signal information. This will be accomplished by the receiver providing two sets of signals shown in Figure 31. Signal A is applied to the

invert control of Figure 25 and controls whether the data link is added or subtracted from the running sum stored in RAM. Signal B is applied to the external reset line on Figure 28. This resets the medium speed counters and stalls the low speed accumulator until the radiometer local oscillator locks up on a new frequency. The high speed sections have been running constantly, thus when Signal B goes low, valid data has already been accumulated in the high speed counters.

Then to provide information pertaining to receiver gain variations, the receiver input is switched from the antenna to a reference source via a waveguide switch. Frequency switching is still maintained while viewing the reference, thus, the reference temperature must be changed between the on and off frequency positions in order not to give a zero result as a reference. The reference information is to be stored separately from the signal information, thus the low accumulation time provides a good division. This would make 2 x 96.5 seconds the minimum switching period. However, since a 50% duty cycle between the antenna and reference source may not be desired, a status bit will be set in order to notify whether the incoming data is signal or reference. This circuitry is shown in Figure 32 and is built on board 2 of the wire-wrap series. Therefore, when the radiometer desires a reference block, it sets the reference line high and waits for a select pulse. On the

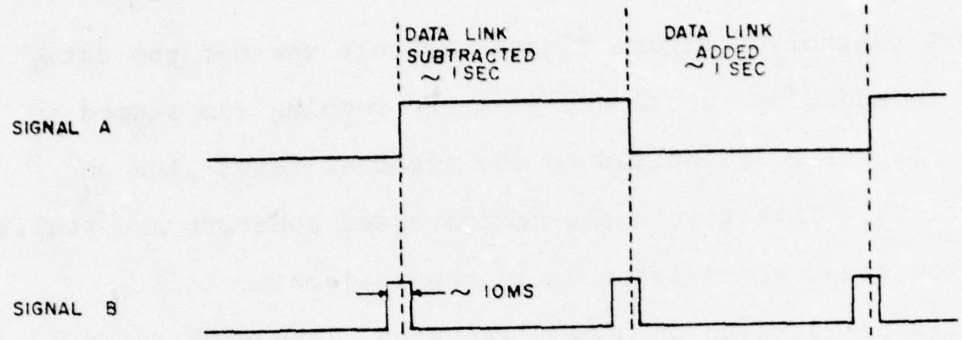

Figure 31. Reference timing

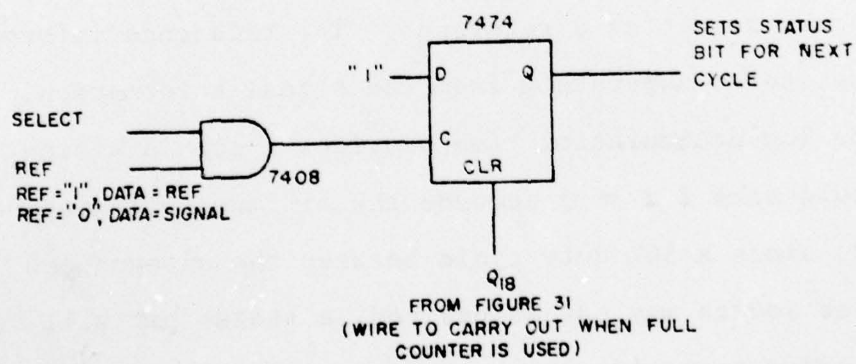

Figure 32. Status generator

rising edge of the select pulse, the external reset line of Figure 28 should be set high. The wave guide switch is then switched and after a setting time, the external reset line is forced low. This process is similar to the nulling action during frequency switching. The status bit then provides the status for the next data set.

The next step is to read sets of data into the Nova. This process is initiated by the $\overline{\text{select}}$ line going high and interrupting the Nova. Actual storage is done by building a memory block in core consisting of the data sets accumulated from each low speed count period. An alternative is to accumulate low speed data sets in Nova core, that is, one data set would be recorded and additional sets would simply be added to the existing set. Software for the former case is given in Appendix D. Finally, the memory block is written on 9 track tape for final reduction by the IBM 370 system.

9.3 <u>Quantization Corrections</u>

The accumulated raw data are now divided by the number of samples taken to give the final "quantized" autocorrelation function. The number of low speed data sets accumulated is the first word of the memory block. Each data set then consists of 16 high speed counts times 2047 medium speed counts. For a 96 second correlation time the medium speed counter is counted 262,144 times, thus, K in Equation (6) is 8,585,740,288.

The resultant "quantized" autocorrelation function is normalized to the zero delay channel and corrected for coarse quantization error. For the zero delay channel, $i=0$ (Equation 13) thus $r(i\Delta\tau)$ and $\rho(i\Delta\tau)$ (normalized corrected autocorrelation function) equals 1. The zero delay channel then represents the total power received. For other channels, $i \geq 1$, $\rho(i\Delta\tau)$ is much less than 1 (Gaussian input uncorrelated) thus $\rho(i\Delta\tau)$ is closer to 1. Equation 14 can be used truncating the terms in Equations 25, 27, 28, and 29 to provide desired accuracy.

9.4 Weighting and Denormalization

Next the normalized autocorrelation function $\rho(i\Delta\tau)$ is multiplied by a weighting function, $w(i\Delta\tau)$. As previously stated, the choice of $w(i\Delta\tau)$ is not critical, and three alternatives are adapted from Weinreb (1965) in Table 2.

A normalized power spectrum, $\rho(i\Delta f)$ is given by the Fourier Transform of $\rho(i\Delta\tau)$. The system gain can then be determined from the reference measurement and incorporated into the signal measurement to provide $\rho(i\Delta f)$ (Equation 7), the actual power spectrum.

AD-A076 018 PENNSYLVANIA STATE UNIV UNIVERSITY PARK F/G 4/1
A HIGH SPEED DIGITAL AUTOCORRELATOR AND ITS APPLICATION TO MESO--ETC(U)
JUL 79 P T PETRUNO , J J OLIVERO DAAG29-78-G-0083
UNCLASSIFIED ERADCOM/ASL-CR-79-0083-1 NL

2 OF 2
AD
A076018

END
DATE
FILMED
12-79
DDC

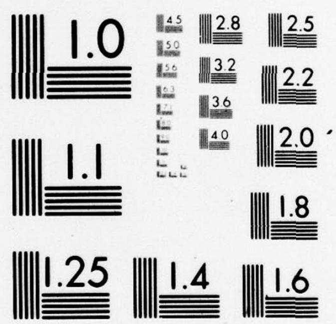

MICROCOPY RESOLUTION TEST CHART
NATIONAL BUREAU OF STANDARDS-1963-A

Table 2. Weighting Functions (after Weinreb, 1963)

Name	Weighting Function $w(n\Delta\tau)$	Fourier Transform $W(f)$	Half Power Bandwidth Δf	Strongest Spurious Response
Uniform	$w(n\Delta\tau) = 1, \lvert n\rvert < N$ $w(n\Delta\tau) = 0, \lvert n\rvert \geq N$	$W(f) = W_o(f) =$ $2N\Delta\tau\frac{\sin 2\pi Nf\Delta\tau}{2\pi Nf\Delta\tau}$	$\frac{0.604}{N\Delta\tau}$	-7db
Cos or Hanning	$w(n\Delta\tau) = 0.5+0.5\cos\frac{\pi n}{N}$ $\lvert n\rvert < N$ $w(n\Delta\tau) = 0, \lvert n\rvert \geq N$	$W(f) = 0.5\ W_o(f)$ $+0.25\ W_o(f+\frac{1}{\Delta\tau 2N})$ $+0.25\ W_o(f-\frac{1}{\Delta\tau 2N})$	$\frac{1}{\Delta\tau N}$	-16db
Blackman	$w(n\Delta\tau) = 0.42+0.5\cos\frac{\pi n}{N}$ $+0.08\cos\frac{2\pi n}{N} \lvert n\rvert < N$ $w(n\Delta\tau) = 0; \lvert n\rvert \geq N$	$W(f) = 0.42\ W_o(f)$ $+0.25\ W_o(f+\frac{1}{\Delta\tau 2N})$ $+0.25\ W_o(f-\frac{1}{\Delta\tau 2N})$ $+0.04\ W_o(f+\frac{1}{\Delta\tau N})$ $+0.04\ W_o(f-\frac{1}{\Delta\tau N})$	$\frac{1.13}{\Delta\tau N}$	-29db

CHAPTER X

EXPERIMENT DURATION

10.1 System Operating Temperature

The length of time during which the experiment is performed is based on the minimum detectable signal as given in Equation (1). In this case, $\alpha=1$ for a full power receiver (Tiuri, 1964), and BW and Top need to be estimated.

Top for a double side band receiver where a signal appears only in one side band is given below (adapted from Okean and Lombardo, 1973):

$$Top = 2(Ta+Te) \tag{40}$$

Where:

Ta = Temperature seen by antenna

Te = Equivalent receiver temperature

Te can be determined by considering Figure 6. Assuming the waveguide switch loss negligible, Te will depend primarily on the mixer-preamplifier noise figure. The mixer-preamp used is a SpaceKom model F22.3V. An RF to IF gain of 34 db will cause noise introduced in succeeding stages to be negligible. Thus, the mixer-preamp broadband double sideband noise figure of 2.6 db will give Te from the following relationship (Mumford and Scheibe, 1968):

$$Te = (F_{DSB}-1)290^{o}K$$

Where:

F_{DSB} = Double sideband noise figure with signal present in both bands (Pure Number)

Te is then equal to 237.7 K. Ta can be approximated from Figures 4 and 5 as 173.64 K and 4336.0 K for the emission and absorption experiments, respectively. Thus, Top for emission and absorption will be 823 K and 9147 K.

10.2 Overall Integration Times

With respect to bandwidth, the system operates as the equivalent of 16 full power receivers since the correlator consists of 16 channels of pure integrators. Thus, τ_I will be considered a pure integration time, and BW will be approximated as 20 MHz/16 or 1.25 MHz.

Other factors influencing τ_I are the time spent viewing reference sources and the loss encountered by resetting the high speed accumulator. Viewing references will reduce τ_I by 1/4, neglecting the relatively short blanking time (Signal B, Figure 37). Skipping 2 of every 18 samples in the high speed accumulator then further reduces the actual time spent correlating to 8/9. A final factor affecting integration time is the quantization error. As previously stated, for the oversampling case, τ_I is effectively reduced by 1/1.43.

By definition, ΔT_{min} of Equation (1) is derived from the idea that the minimum detectable signal is equal to the

standard deviation of the received power (Tiuri, 1964). In practice, however, the minimum detectable signal should be made 1/4 of the received power's standard deviation. This new value of ΔT_{min} will minimize the probability of random noise being interpreted as signal (Tiuri, 1964). However, from the original design criteria, signal detection is not sufficient. An accurate representation of spectral line shape was originally specified. The overall accuracy will now be defined as 1% of the signal amplitude limited, of course, to the 16 equally spaced spectral points. Thus, ΔT_{min}'s of 0.005 K and 0.30 K, for the emission and absorption experiments, respectively (from Figures 4 and 5), will provide reasonable minimum integration times.

Equation (1) now becomes:

$$\Delta T_{min} = \frac{Top}{[(1.25\text{x}10^6 H_z)(\tau_I)(4)(9/8)(1.43)]^{1/2}} \qquad (42)$$

For the emission experiment, τ_I becomes approximately 3400 seconds and for absorption, 115 seconds.

CHAPTER XI

CONCLUSIONS

11.1 System Choice

In this study, a system is described that will detect stratospheric and mesospheric water vapor. The method of detection involves a remote measurement of the molecular absorption or emission spectrum. The resultant spectral data can then be used to determine water vapor mixing ratios versus altitude by inverting the radiative transfer equation. The accuracy of this type of measurement is heavily dependent on spectral line shape, thus much of this study concerns a system capable of accurate spectral measurement.

The system consists of a 22 GHz receiver feeding a 20 MHz bandwidth spectral analyzer. The emphasis then is placed on the design of a suitable spectral analyzer of which two types were considered. These were a discrete filter bank and an autocorrelator in both analog and digital forms. With design considerations of stability, sensitivity, resolution, complexity, and cost, a 1 x 2 bit digital autocorrelator was chosen as the best overall system.

11.2 System Design

Sampling at the Nyquist rate is adequate in multibit systems. However, for a hard quantization scheme, as is the case here, system sensitivity is reduced but can be partly

recovered by sampling at twice the Nyquist rate (80 Mhz). Also, a further increase of the sampling rate to 100 MHz will allow adjustment of the resultant frequency centers without decreasing sensitivity.

The autocorrelation and first accumulation are then constructed on printed circuit boards using the ECL 10,000 logic series. A medium speed accumulator is then also constructed on printed circuit boards using both Schottky and standard TTL logic. A final low speed accumulator and computer interface is then wire wrapped using MOS and TTL logic. All further data reduction, including a discreet Fourier Transform and spectrum denormalization, is performed in software.

11.3 Suggestions for Future Work

At the time of this writing, a prototype system consisting of 16 autocorrelation points was designed, two points of which were built. An immediate goal then is to complete the 16 points and use the system for a ground based measurement.

To complement the hardware system, a software package can be constructed to perform various tasks. For instance, different types of Fourier Transforms (FFT, Chirp-Z) can be programmed to allow grouping or spreading of spectral points. Also, overall teletype control and real time displays would enhance system operation.

Extended goals would be to perform an intra-atmosphere measurement from a balloon. Such a system would require a telemetry link to ground and could also provide real time results. A third alternative is a "look down" experiment, that is, a measurement from outside the earth's atmosphere. This type of measurement might be performed in the 1980's as part of a Space Shuttle experiment.

APPENDIX A

TRUNCATION ERROR

Quantifying the error introduced from truncating counter bits can be handled by considering the effects of variance on the total resultant counts. Ables, et al. (1974) handled a similar truncation problem by adding a "round off" variance to the full counter variance. Here then, dividing the difference between the full counter plus rounded counter variance and the full counter variance by the full counter variance will provide a relative indication of the change in overall variance.

The rounding error (variance) is given by $\sigma_{er}^2 = V^2/12$ where V is the value of the least significant bit used. The probability, p, of counts occurring is given by the numerator of Equation (14), used in conjunction with Equations (30) through (33). The variance of a full digit counter is then $\sigma_{FL}^2 = P(1-P)N$, where N is the total number of samples. The relative variance is:

$$\sigma_{REL}^2 = \frac{[P(1-P)N+V^2/12]-P(1-P)N}{P(1-P)N} \tag{A1}$$

$$\sigma_{REL}^2 = \frac{V^2}{24[\frac{Z(V_o)}{\sqrt{2\pi}} + n^{-1}(\frac{1}{2\pi} - \frac{Z(V_o)}{\sqrt{2\pi}})]\rho N} \tag{A2}$$

Using V_o=0.95, N=4, and $V=2^3$:

$$\sigma^2_{REL} = \frac{23.02}{\rho N} \tag{A3}$$

Obviously then, for loosely correlated signals, as is the case here, N will need to be extremely large in order to provide an insignificant change in system sensitivity due to bit truncation. Thus, if the incoming signal is assumed very loosely correlated, say $\rho \approx 0.0001$, then an N on the order of 10^8 is necessary to reduce the change in variance to 0.1%. However, at a 100 MHz sampling rate, 10^8 samples occur every second. Therefore, the truncation error can be ignored for correlation time on the order of seconds or longer.

APPENDIX B

TIMING DIAGRAMS

Following are expected waveforms from throughout the system. Note these waveforms are of two types, one describing actual signal levels and the other describing whether data are valid or not. The "data valid" waveforms will be labeled in parenthesis and will indicate data valid as high, invalid as low. The signal level waveforms are labeled without parenthesis and represent a logical one when high, a zero when low.

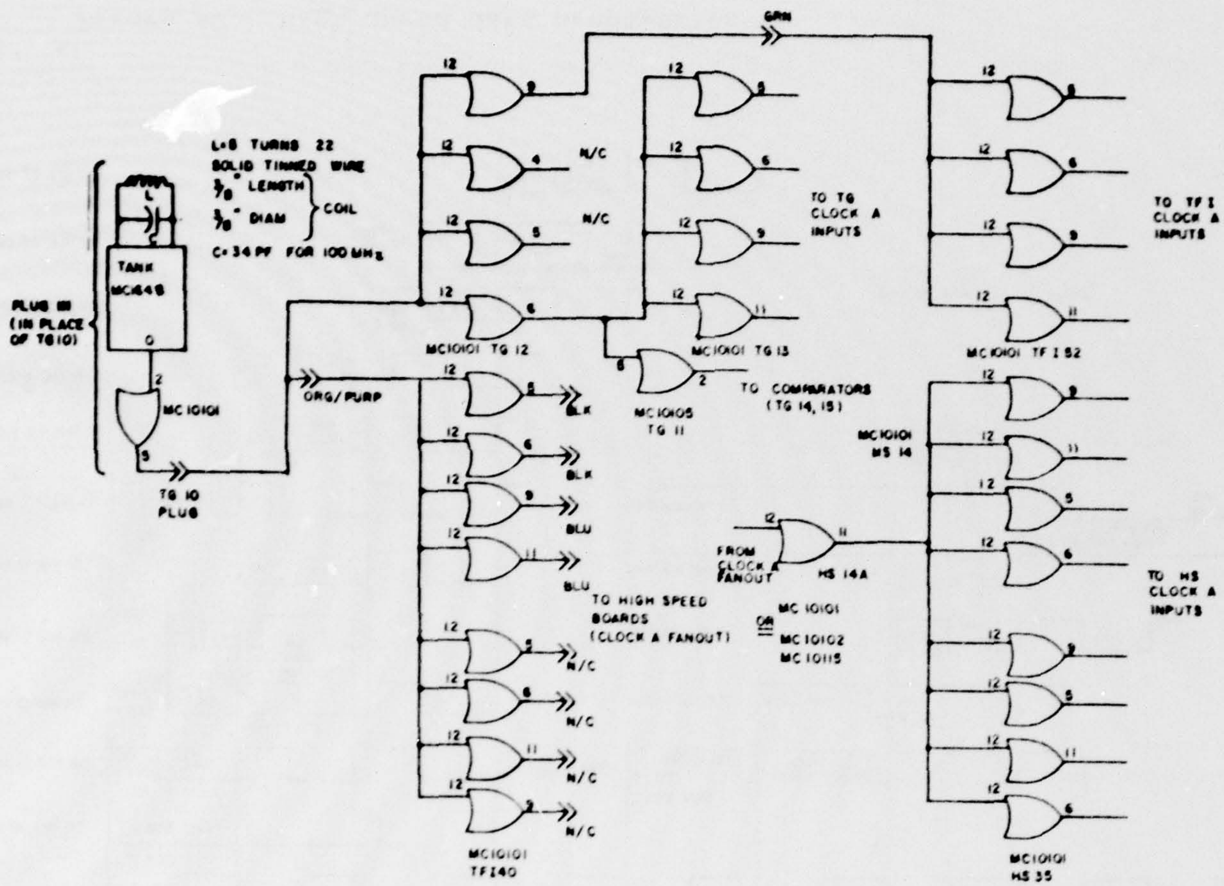

Figure A1. Clock A distribution

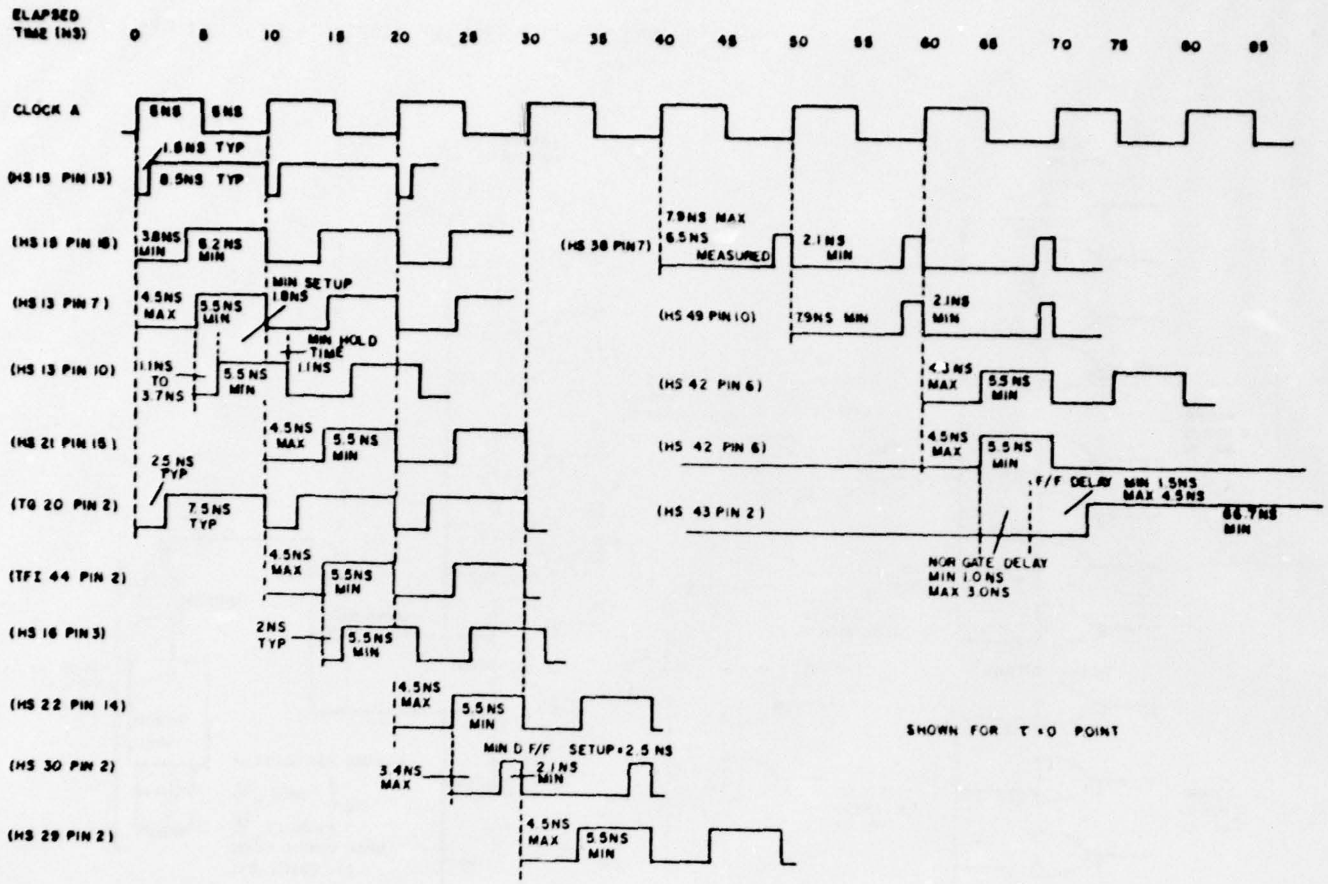

Figure A2. High speed data propagation

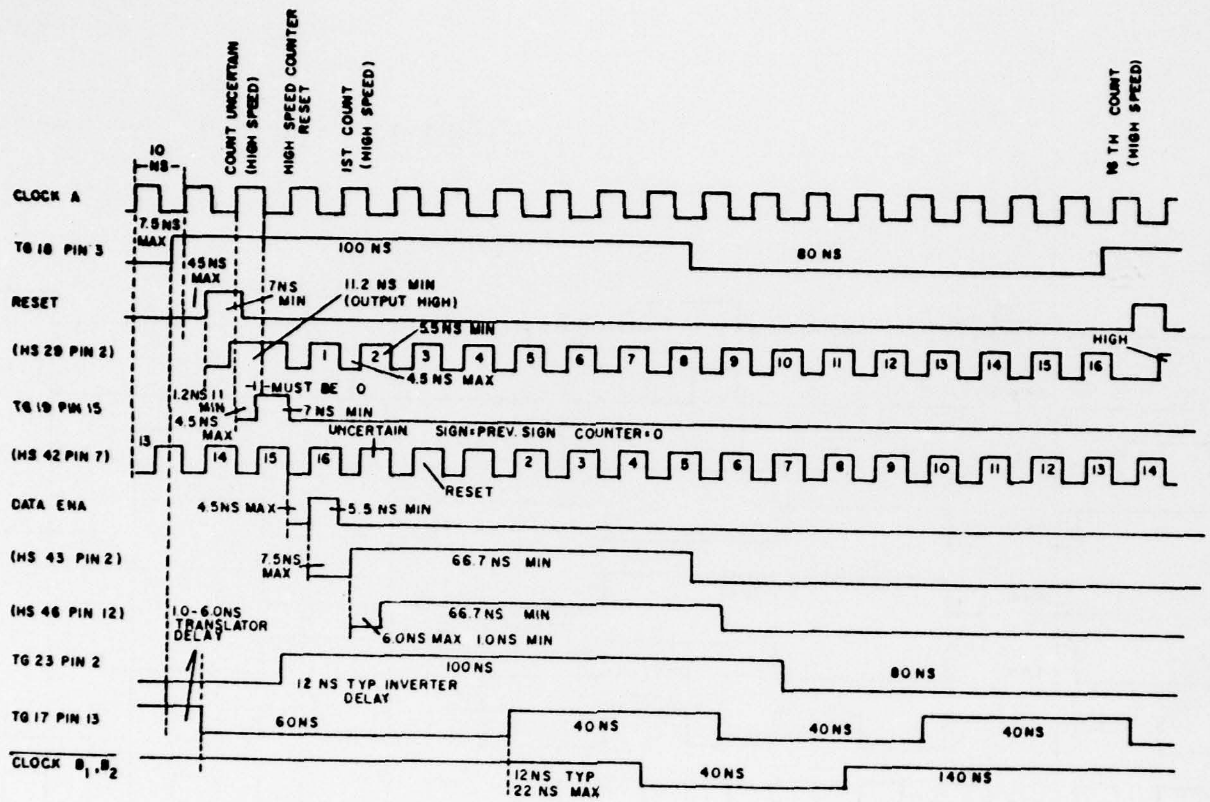

Figure A3. High to medium speed transition

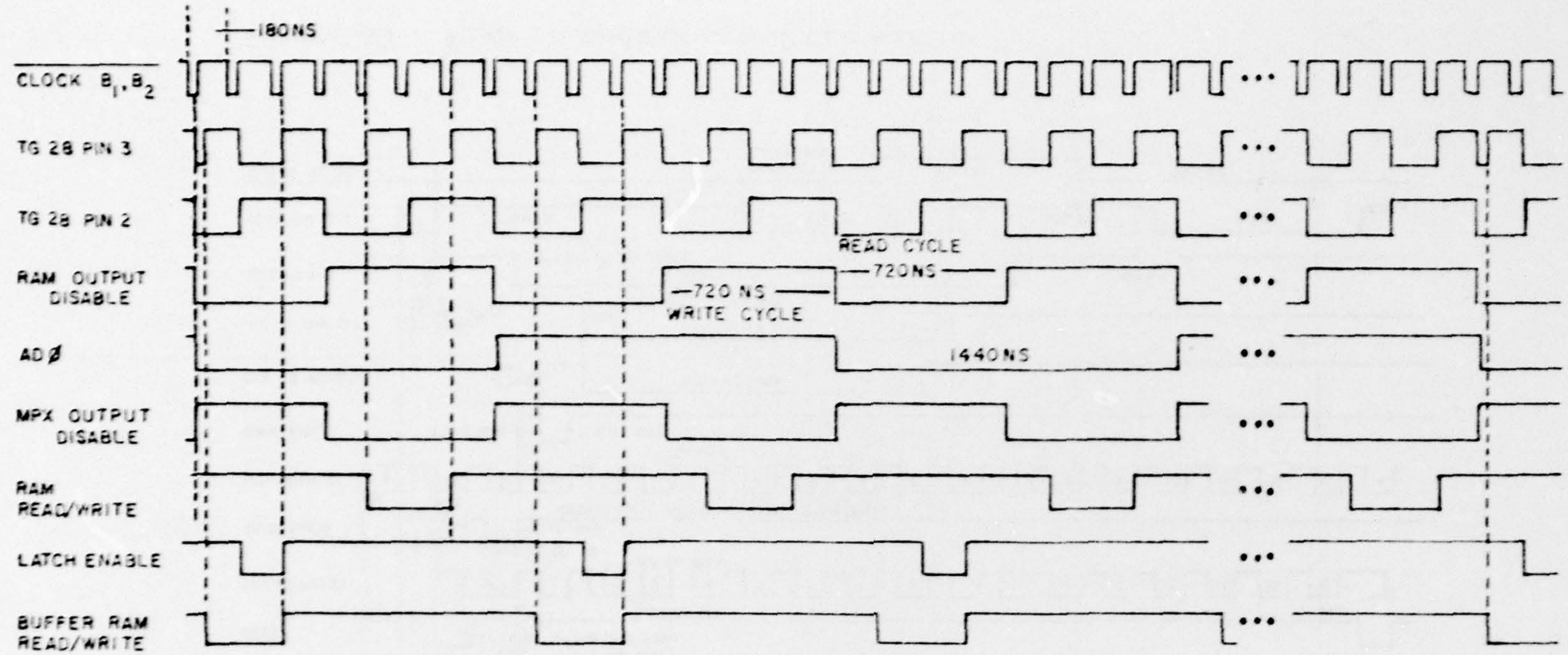

Figure A4. Low speed timing

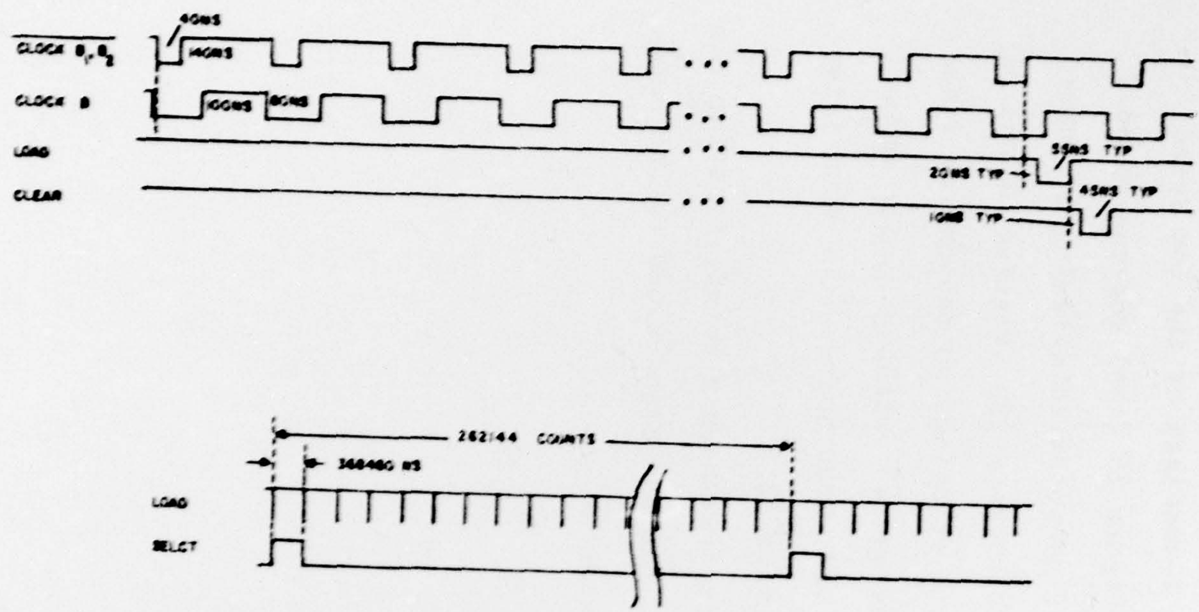

Figure A5. a) Load/clear generation; b) Select generation

APPENDIX C

WIRE WRAP BOARDS

Shown here are the physical layouts of the two wire wrap boards. Board 1 consists of the low speed accumulator as shown in Figure 26 (top) whereas Board 2 consists predominantly of computer interfacing circuitry (bottom of Figure 26) and bookkeeping (Figures 30 and 31).

At the time of this printing, no radiometer interfacing circuitry was constructed, although ample space was available on either wire wrap board. One such interface was presented in Figure 33.

Also included here are the pin connections for the two wire wrap boards and the bus connections to the Data General Nova 1200 minicomputer.

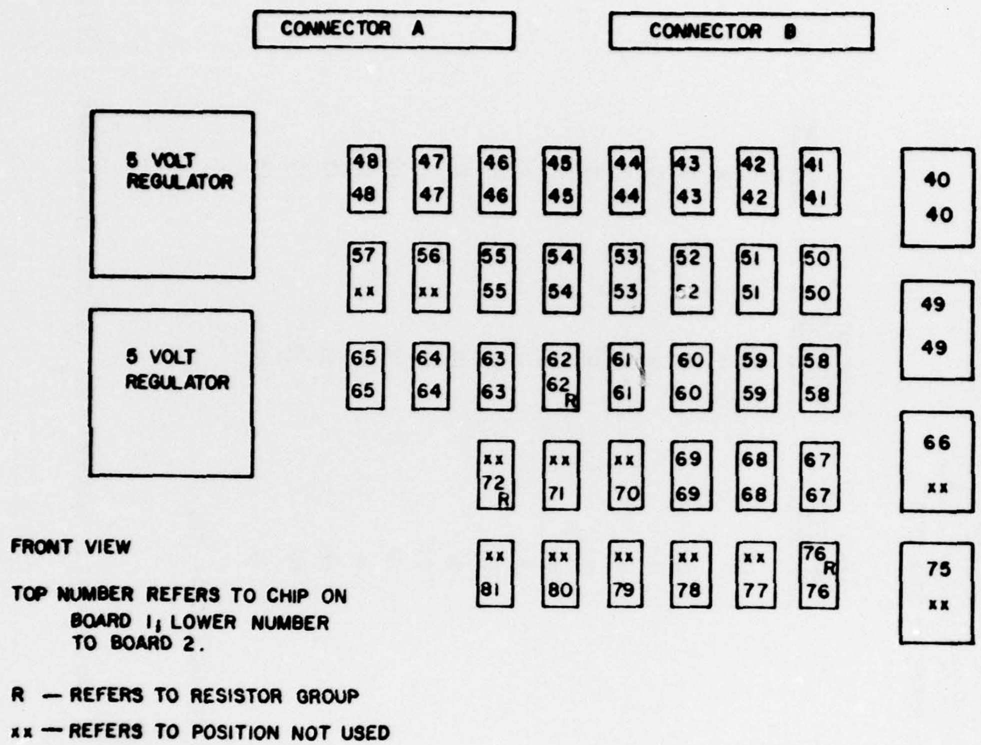

Figure A6. Wire wrap physical layout

NOVA RACK FRONT VIEW

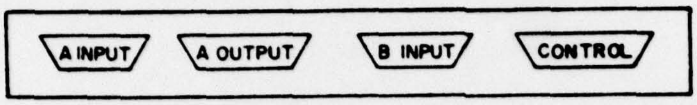

CONNECTOR FRONT VIEW

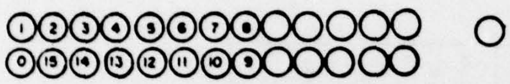

(NUMBERS REFER TO DATA BITS)

DATA BIT	INPUT CONNECTOR NUMBER	OUTPUT CONNECTOR NUMBER	CONTROL
0	14	25	15
1	1	13	8
2	2	12	7
3	3	11	6
4	4	10	5
5	5	9	4
6	6	8	3
7	7	7	2
8	8	6	1
9	21	18	X
10	20	19	9
11	19	20	10
12	18	21	11
13	17	22	12
14	16	23	13
15	15	24	14

DATA INTERFACE DEVICE CODE : 72_8

Figure A7. Nova data interface (after Sweitzer, 1978)

Wire wrap Board 1, Connector A

A1	GND	AA	DB0 (LSB)
A2	+7 v. unreg.	AB	DB1
A3		AC	DB2
A4	A0 (LSB)	AD	DB3
A5	A1	AE	DB4
A6	A2	AF	DB5
A7	A3	AH	DB6
A8	A4	AJ	DB7
A9	A5	AK	DB8
A10	A6	AL	DB9
A11	A7	AM	DB10
A12	RAM READ/WRITE	AN	DB11
A13	RAM OUTPUT DISABLE	AP	DB12
A14		AR	DB13
A15		AS	DB14
A16		AT	DB15
A17		AU	DB16
A18		AV	DB17
A19		AW	DB18
A20		AX	DB19
A21		AY	DB20
A22		AZ	DB21

Wire wrap Board 2, Connector A

A1	Ground	AA	A0 (LSB)
A2	+7 v. unreg.	AB	A1
A3	CAD 0 (LSB)	AC	A2
A4	CAD 1	AD	A3
A5	CAD 2	AE	A4
A6	CAD 3	AF	A5
A7	CAD 4	AH	A6
A8	CAD 5	AJ	A7
A9	CAD 6	AK	CH1
A10	CAD 7	AL	CH2
A11	CAD 8	AM	CH3
A12	LOAD	AN	CH4
A13	DB0 (LSB)	AP	CH5
A14	DB1	AR	CH6
A15	DB2	AS	CH7
A16	DB3	AT	CH8
A17	DB4	AU	CH9
A18	DB5	AV	CH10
A19	DB6	AW	CH11
A20	DB7	AX	CH12
A21	DB8	AY	CH13
A22	DB9	AZ	CH14

Wire wrap Board 1, Connector B

B1		BA	DB22
B2		BB	DB23
B3		BC	DB24
B4		BD	DB25
B5		BE	DB26
B6		BF	DB27
B7		BH	DB28
B8		BJ	DB29
B9		BK	DB30
B10		BL	DB31
B11	DL0 (LSB)	BM	
B12	DL1	BN	
B13	DL2	BP	
B14	DL3	BR	
B15	DL4	BS	
B16	DL5	BT	
B17	DL6	BU	
B18	DL7	BV	
B19	DL8	BW	INVERT CONTROL
B20	DL9	BX	MPX OUTPUT ENABLE
B21	DL10	BY	SELECT
B22	DL11	BZ	LATCH ENABLE

Wire wrap Board 2, Connector B

B1	DB10	BA	CH15
B2	DB11	BB	CH16
B3	DB12	BC	BUFFER RAM READ/
B4	DB13	BD	WRITE
B5	DB14	BE	SELECT
B6	DB15	BF	START
B7	DB16	BH	CDB0 (LSB)
B8	DB17	BJ	CDB1
B9	DB18	BK	CDB2
B10	DB19	BL	CDB3
B11	DB20	BM	CDB4
B12	DB21	BN	CDB5
B13	DB22	BP	CDB6
B14	DB23	BR	CDB7
B15	DB24	BS	CDB8
B16	DB25	BT	CDB9
B17	DB26	BU	CDB10
B18	DB27	BV	CDB11
B19	SB28	BW	CDB12
B20	DB29	BX	CDB13
B21	DB30	BY	CDB14
B22	DB31	BZ	CDB15

APPENDIX D

NOVA SOFTWARE

Presented here is the software routine enabling data to be stored in the Data General Nova 1200 minicomputer. Data are stored in the form of 32 bit words, forming a memory block, beginning at location 200_8. The higher order 16 bits of a word are stored first (lower memory location). The first word of the memory block provides the number of 17 word cycles recorded in the block. Next, the first word of a cycle is recorded, providing the status of that cycle. A 1073741824 (bit 2^{30} set) indicates signal data and a 3221225472 (bits 2^{30} and 2^{31} set) indicates reference data. Finally, 16 data words are recorded, beginning with zero lag point. The 17 word cycles are then repeated until termination of the experiment.

The program operates as an interrupt service routine, that is, the program sits in a loop in between the 17 word cycle recordings. A $\overline{\text{select}}$ pulse then interrupts the loop and a cycle of data is recorded. Upon reception of a zero status word, the program is terminated.

For transfer to the IBM 370 system, the Nova can record the data block directly on 9 track tape, location 200_8 first. Then, using Fortran IV, the IBM system can directly form 10 bit (I4) integers.

The Nova software shown here is in assembled form and, thus, the complete assembler numonics are not given.

Interrupt Service

0		PC	PC during interrupt
1		000002	Go to 2
2	SKPD2	063772	Skip if device 72 not interrupting
3	JMP	000076	Service device 72
4	HALT	063277	Halt
5	JMP	000073	Jump to 73

Registers

22	Memory block address (indexed)
40	Status address
41	200_8 stored
201	No. of cycles recorded
43	32_{10} stored
44	Cycle addr
45	Skip 1st cycle word

Start - initialize registers — Set PC to 50

50	INTDS	060277	Interrupt disabled
51	SUBO	126440	Clear AC1
52	STA	044201	Clear 201
53	STA	044045	Clear 45
54	STA	044200	Clear 200
55	INC	125500	Inc ACL and shift left
56	MOV	125120	Shift AC1 left
57	MOV	125120	Shift AC1 left
60	MOV	125120	Shift AC1 left
61	MOV	125120	Shift AC1 left
62	STA	044043	Store 32_{10} in 43
63	MOV	125120	Shift AC1 left
64	MOV	125120	Shift AC1 left
65	STA	044041	Store 200_8 in 41
66	INC	125400	Increment AC1
67	STA	044022	Store 201_8 in 22
70	SUBO	126440	Clear AC1
71	MOV	125240	Set carry=1, shift right
72	STA	044040	Store status addr in 40

Wait for data loop

73	INTEN	060177	Interrupt enabled
74	NIO	060000	No operation
75	JMP	000777	Jump back 1

Skip initial cycle

76	LDA	024045	Load 1st cycle word into AC1
77	MOV	125025	Skip if AC1 non-zero
100	JMP	000127	Ignore 1st cycle

Initialize address counter

101	LDA	024043	Load 32_{10} into AC1
102	STA	044044	Store AC1 in 44

Receive cycle status (Ref/sig) - Experiment complete if status word = 0

103	LDA	024040	Load status addr onto AC1
104	DOA	065072	Send status addr
105	DIB	065472	Receive status addr onto AC1
106	MOV	125025	Skip on status non zero
107	JMP	000132	Jump to tape routine
110	STA	046022	Store status in memory block
111	SUBO	126440	Clear AC1
112	STA	046022	Store blank in memory block

Record 32 words

113	INC	125400	Increment AC1
114	INC	125400	Increment AC1
115	DOA	065072	Send addr
116	DIA	070472	Receive data in AC2
117	STA	052022	Store data in memory block
120	DSZ	014044	Decrement 44, skip if zero
121	JMP	000773	Jump back 5

Record no cycles completed, clear interrupt conditions, return to wait loop

122	ISZ	010201	Increment cycles recorded
123	JMP	000402	Jump ahead 2
124	HALT	063277	Halt if no. cycles $\geq 2^{16}$
125	NIO	060272	Clear busy and done on device 72
126	JMP	000073	Jump to 73

Skip initial cycle routine, clear interrupt conditions, return to wait box

127	ISZ	010045	Increment 1st cycle word
130	NIO	060272	Clear busy and done on device 72
131	JMP	000073	Jump to 73

Record number of cycles in front of memory block

132	LDA	020042	Load no. cycles onto AC0
133	STA	042041	Store AC0 on 201

Set up number of words to read on tape

134	LDA	020201	Load cycle count into ACO
135	LDA	024201	Load cycle count into ACO
136	LDA	034043	Load 32_{10} in AC3
137	MOV	175220	Shift AC3 right
140	MOV	125122	Shift AC1 left, skip on zero carry
141	HALT	063277	No. cycles $\geq 2^{10}$
142	MOV	175223	Shift AC3 right, skip if carry = 1
143	JMP	000775	Jump back 3
144	MOV	101120	Shift ACO left
145	ADD	107022	Add ACO and AC1, skip if carry = 0
146	HALT	063277	Number of words too big
147	INC	125422	INC AC1, skip if carry = 0
150	HALT	063277	Number of words too big
151	INC	125422	INC AC1, skip if carry = 0
152	HALT	063277	Number of words too big

REFERENCES

Ables, J. G., Cooper, B. F. C., Hunt, A. J., Moorey, G. G., and Brooks, J. W., "A 1024-Channel Digital Autocorrelator," Review of Scientific Instruments, Vol. 46, No. 3, pgs. 284-295, 1975.

Blackman, R. B., and Tukey, J. W., The Measurement of Power Spectra, Dover Publications, Inc., New York, 1958.

Botos, B., "Nanosecond Pulse Handling Techniques in I/C Interconnections," Motorola Integrated Circuit Technical Information Note, AN-270.

Brown, R. G., Sharpe, R. A., Hughes, W. L., and Post, R. E., Lines, Waves, and Antennas, The Ronald Press Co., New York, 1973.

Burus, W. R., and Yao, K. S., "Clipping Loss in the One Bit Autocorrelation Spectral Line Receiver," Radio Science, Vol. 4, No. 5, pgs. 431-436, 1969.

Cooper, B. F. C., "Correlators with Two-Bit Quantization," Australian Journal of Physics, Vol. 23, pgs. 521-527, 1970.

Dicke, R. H., "The Measurement of Thermal Radiation at Microwave Frequencies," Review of Scientific Instruments, Vol. 17, pgs. 268-275, 1946.

Dwight, H. B., Tables of Integrals and Other Mathematical Data, The MacMillian Co., New York, 1947.

Hagan, J. B., and Farley, D. T., "Digital-Correlation Techniques in Radio Science," Radio Science, Vol. 8, Nos. 8,9, pgs. 775-784, 1973.

Harming, R. W., Digital Filters, Prentice Hall, Inc., Englewood Cliffs, New Jersey, 1977.

Jaeger, R., "ECL 10,000 Interconnects Economically," Electronic Design, Vol. 22, No. 20, pgs. 90-94, 1974.

Klopper, H., "Sensitivity of Crystal Video Receivers with RF Pre-Amplification," The Microwave Journal, Vol. 8, No. 8, pgs. 85-92, 1965.

Lewis, J. B., Linear Dynamic Systems, Matrix Publishers, Inc., Champaign, Illinois, 1977.

Longbothum, R. L., "A Study of Water Vapor Measurement in the Stratosphere and Mesosphere Using Microwave Techniques," Scientific Report 449, Ionosphere Research Laboratory, The Pennsylvania State University, University Park, Pennsylvania, 1976.

Longbothum, R. L., personal communication, 1977.

Meeks, M. L., Editor, Methods of Experimental Physics, Vol. 12, Astrophysicas Part B: Radio Telescopes, Academic Press, New York, 1976.

Motorola Semi-Conductor Products, Inc., Semi-Conductor Data Library, MECL Integrated Circuits, Vol. 4, Series A, 1974.

Mumford, W. W., and Scheibe, E. H., "Noise Performance on Communication Systems," Horizon House-Microwave, Inc., Dedham, Massachusetts, 1968.

National Bureau of Standards, Handbook of Mathematical Functions, Applied Mathematics Series, No. 55, pgs. 927-949, 1964.

Okean, H. C., and Lombardo, P. P., "Noise Performance of M/us and MM-Wave Receivers," Microwave Journal, Vol. 16, No. 1, January 1973.

Oppenheim, A. V., and Schafer, R. W., "Digital Signal Processing," Prentice-Hall, Inc., Englewood Cliffs, New Jersey, 1975.

Pell, C., and Little, L. T., "A High Speed Digital Autocorrelation Spectrometer for Millimeter Astronomy," Journal of Physics E: Scientific Instruments, Vol. 8 pgs. 786-789, 1975.

Rabiner, L. R., and Gold, B., "Theory and Application of Digital Signal Processing," Prentice-Hall, Inc., Englewood Cliffs, New Jersey, 1975.

Schwartz, M., and Shaw L., "Signal Processing: Discrete Spectral Analysis, Detection and Estimation," McGraw-Hill Book Co., 1975.

Sweitzer, K. R., personal communication, 1978.

Texas Instruments, Inc., The TTL Data Book, 2nd Edition, 1976.

Tiuri, M. E., "Radio Astronomy Receivers," IEEE Transactions on Antennas and Propagation, Vol. AP-12, No. 7, pgs. 930-938, 1964.

Waters, J. W., "Absorption and Emission by Atmospheric Gases," Methods of Experimental Physics, Vol. 12 Astrophysics, Part B: Radio Telescopes, Academic Press, 1976.

Weinreb, S., "A Digital Spectral Analysis Technique and Its Application to Radio Astronomy," Technical Report 412, Research Laboratory of Electronics, Massachusetts Institute of Technology, 1963.

☆ U.S. GOVERNMENT PRINTING OFFICE: 1979 — 677-017/25